NJC

ROYAL SOCIETY OF CHEMISTRY

PERSPECTIVE

View Article Online
View Journal | View Issue

Cite this: *New J. Chem.*, 2021, **45**, 20046

Name reactions: strategies in the design of chemodosimeters for analyte detection

Anwesha Maiti,[a] Saikat Kumar Manna,[b] Dipanjan Banik[a] and Ajit Kumar Mahapatra *[a]

Received 24th August 2021,
Accepted 1st October 2021

DOI: 10.1039/d1nj04056a

rsc.li/njc

The design and synthesis of suitable chemodosimeters for the detection of toxic analytes has become challenging for new researchers nowadays in the molecular recognition field. Among different chemical reactions, name reaction-based approaches will help researchers to gain knowledge about different types of name reactions for different analytes, the mechanism of sensing using these reactions, the names of scientists who pioneered these name reactions, and also to explore unknown name reactions for unexplored analytes. In this context, we have reported different sensing strategies, *i.e.*, name reaction-based approaches involved in designing various chemodosimeters during the past decades. The name reaction-based approaches have been classified into 11 types, such as (a) Tsuji–Trost allylic cleavage, (b) Suzuki–Miyaura coupling, (c) Claisen rearrangement, (d) benzil-cyanide reaction, (e) intramolecular crossed-benzoin reaction, (f) Michael addition reaction, (g) Gabriel mechanism, (h) 2-aza-Cope rearrangement, (i) Baeyer–Villiger reaction, (j) Beckmann rearrangement, and (k) Lossen rearrangement. The focus of the review is mainly on how name reactions are used in analyte detection chemodosimetrically.

1. Introduction

Supramolecular chemistry is an interdisciplinary area, enticing not just chemists but also biologists, biochemists, physicists, environmentalists, theoreticians, and a wide range of other researchers. It is one of the most attractive and rapidly developing fields of chemistry, and its research encompasses a variety of processes that are monitored by particular non-covalent interactions between molecules. Charles J. Pedersen, Jean-Marie Lehn, and Donald J. Cram shared the Nobel Prize in Chemistry in 1987 for their achievements in the invention and application of supramolecular chemistry.[1–5] One of the key terms used frequently with supramolecular chemistry is

[a] *Department of Chemistry, Indian Institute of Engineering Science and Technology, Shibpur, Howrah 711103, West Bengal, India. E-mail: akmahapatra@chem.iiests.ac.in*
[b] *Department of Chemistry, Haldia Government College, Debhog, Haldia, Purba Medinipur 721657, West Bengal, India*

Anwesha Maiti

Anwesha Maiti earned her BSc honours degree in chemistry from Midnapore College, affiliated to Vidyasagar University, in 2014. She obtained her MSc degree from Indian Institute of Engineering Science and Technology, Shibpur, Howrah, in 2016. Currently, she is working as a research scholar at the Department of Chemistry, IIEST, Shibpur under the supervision of Prof. Ajit Kumar Mahapatra.

Saikat Kumar Manna

Dr Saikat Kumar Manna received his PhD degree (2015) from Indian Institute of Engineering Science and Technology, Shibpur, Howrah. He is currently an Assistant Professor at the Postgraduate Department of Chemistry, Haldia Government College, West Bengal, India. His research activity primarily focuses on the development of fluorescent probes (chemosensors/chemodosimeters) for the detection of various analytes and bioimaging. To date, he has authored 37 scientific publications.

molecular recognition.[6,7] The concept of molecular recognition emerges from the specific interactions between two or more molecules such as H-bonding, metal-coordination, hydrophobic forces, van der Waals forces, π–π interactions, and electrostatic forces, by which molecules can recognize each other.[8,9] In the last two decades, various receptors have been designed for understanding molecular recognition. The roots of molecular recognition lie in host–guest interaction.[10,11] The host is similar to a lock, in which the key fits perfectly. Now, the terminology chemosensor is more closely connected with a molecular event in host–guest chemistry. The indicator is known as a chemosensor if the particular binding interaction between the host and the guest is noncovalent and reversible, and the interaction may be disturbed under certain variables.[12–14] However, the indicator is referred to as a chemodosimeter if the binding relationship between the host and the guest is totally based on highly-selective irreversible chemical reactions.[15,16] The term chemodosimeter was coined by Chae and Czarnik to describe an abiotic molecule that can recognize analytes while also transduction a visible signal in an irreversible manner.[17–19] The host–guest interactions between the chemodosimeter and analyte trigger these chemical processes, which results in the formation or breaking of covalent bonds instead of the generation of supramolecular complexes. Because of the structural alterations caused by the chemical reaction, such chemodosimeters have better selectivity, sensitivity, and excellent photophysical properties changes compared to chemosensors, which are mainly based on noncovalent interactions.[20] The design of suitable chemosensors/chemodosimeters for a particular analyte are now a great challenge to us in the molecular recognition field. An ideal chemosensor/chemodosimeter should elicit a change in the color/fluorescence to naked eyes upon interaction with the analyte. Thus, it is very much important to understand the molecular interactions. In the past years, various types of chemosensors/chemodosimeters for charged (anions and cations) and neutral analytes have been developed.[21–25] Moreover, chemodosimeter design, synthesis, and application in analyte detection have drawn growing attention and become a very active area of research due to their quick reaction, good resistance in aqueous conditions, high sensitivity, and good selectivity. Chemodosimeters are generally made up of at least two functioning units: (a) one is the reaction site, where the host interacts with the analyte, and (b) the second is the signaling unit, whose characteristics must change upon interaction with the target analyte (Scheme 1). In the past few years, many fluorescent probes have been described for the chemodosimetric detection of several analytes *via* selective name chemical reaction and additive signalling mechanisms. The name chemical reactions implemented for sensing several analytes are Tsuji–Trost allylic cleavage, Suzuki–Miyaura coupling, Claisen rearrangement, benzil-cyanide reaction, Intramolecular crossed-benzoin reaction, Michael addition,

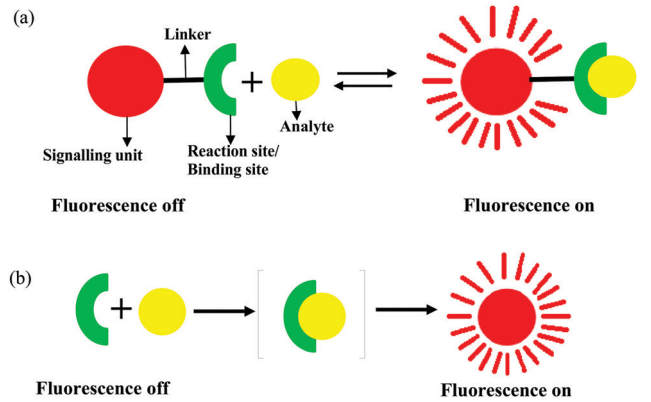

Scheme 1 Schematic presentation of (a) chemosensor and (b) chemodosimeter.

Dipanjan Banik

Mr Dipanjan Banik obtained his Bachelor's degree with honours in chemistry from Vidyasagar University in 2016, followed by his Master's degree from the same university in 2018. He is presently working towards his doctoral degree under Professor Mahapatra's supervision at Indian Institute of Engineering Science and Technology, Shibpur, Howrah.

Ajit Kumar Mahapatra

Ajit Kumar Mahapatra is a Sr. Professor of Chemistry at the Indian Institute of Engineering Science and Technology, Shibpur, Howrah. He received his PhD degree in 2001 from Bengal Engineering and Science University, Shibpur, Howrah (presently, IIEST, Shibpur). He has published over 100 research articles in peer-reviewed international journals in the area of supramolecular chemistry, molecular recognition, and synthetic organic chemistry. So far, his publications have received 1518 citations. His present research interests include the development of modern techniques such as organic thin film (OTF) substrate-based colorimetric and fluorimetric chemosensors for the estimation of environmentally and biologically relevant toxic molecules, metal ions, as well as anions.

Gabriel mechanism, 2-aza-Cope Claisen rearrangement, Baeyer–Villiger reaction, Beckmann rearrangement, and Lossen rearrangement. Tsuji–Trost allylic cleavage, Suzuki–Miyaura coupling, and Claisen rearrangement are involved in palladium recognition. Various important name reactions are used to detect anionic analytes, such as the benzil rearrangement and intramolecular crossed-benzoin reaction for CN^-, and the Michael addition for CN^-. Name reactions for neutral analytes, *i.e.*, Gabriel mechanism for N_2H_4 recognition, 2-aza-Cope rearrangement for HCHO sensing, Michael reaction for biothiols, Baeyer–Villiger reaction for H_2O_2, Beckmann rearrangement for $COCl_2$, and Lossen rearrangement for DCP sensing have been reported in the literature.

In this review, we will briefly introduce selected examples of fluorescent chemodosimeters characterized by different types of name reactions implemented at the molecular recognition site for toxic analytes (Pd^0, Pd^{2+}, CN^-, N_2H_4, HCHO, biothiols, H_2O_2, $COCl_2$, and DCP) detection. In addition, design strategies, sensing processes, and applications of related fluorescent chemodosimeters are also addressed here in detail. Moreover, the directions for the future of research on the topic will be briefly discussed. To the best of our knowledge, to date, there have been no comprehensive studies that explain the progress and processes of name reaction-based sensors. The aim of this study is to offer a broad overview of the idea and development of chemodosimeters based on name reactions, as well as to encourage researchers for future research investigations in this promising subject.

2. Name reactions

2.1. Tsuji–Trost allylic cleavage

The Tsuji–Trost reaction[26] is a palladium-catalyzed π-allyl substitution reaction where a leaving group in the allylic position of a substrate is replaced by a nucleophile. Jiro Tsuji was the pioneer of the above reaction and later Barry Trost adapted this reaction in 1973 by introducing phosphine ligands. In this reaction mechanism, palladium at first underwent the oxidative addition reaction by coordinating with the allyl moiety to form the π-allyl complex, which was subsequently attacked by a nucleophile to form the substituted product (Scheme 2). Using this reaction heterocyclic ring, the heterocyclic indole derivatives can be synthesized through the formation of an intramolecular π-allyl complex and this reaction mainly gives an allylic nucleophilic substituted product. This type of reaction has been extensively used for the design of various fluorescent probes for Pd^{2+} recognition.

In 2014, Zhu and coworkers reported an NIR-based ratiometric fluorescent probe **1** for imaging palladium within live cells based on Tsuji–Trost allylic cleavage.[27] On the addition of $Pd(PPh_3)_4$ to the PBS–CH_3CN (3 : 1, pH = 7.4, 0.01 M) mixture solution, the absorption band at 810 nm gradually decreased and a new band appeared at 545 nm with a clear isosbestic point at 640 nm. The color of the solution changed from light green to red, which was clearly observable by the naked eye. The observed color change was due to palladium-triggered allylic carbamate bond cleavage that disrupted the extended conjugation and reduced the conjugated chain length in its keto derivative (Fig. 1). The absorbance ratio of $A_{545\,nm}/A_{810\,nm}$ showed a good linear relationship with the palladium concentration. Upon the gradual addition of $Pd(PPh_3)_4$, a gradual decrease in emission intensities at 825 nm and, concurrently, a significant enhancement of emission intensities at 655 nm, were observed. The main reason behind the changes in the probe's optical nature was due to the removal of the masking group chloroformate by palladium. ^1H NMR and mass spectroscopy were used to monitor the reaction between probe **1** and palladium. Probe **1** displayed a ratiometric fluorescence color change from green to red with an enhancement in the fluorescence intensity of about 130-fold at 655 nm. The fluorescence intensity ratio of $I_{655\,nm}/I_{825\,nm}$ showed a good linear relationship with $[Pd^{2+}]$ over a wide range of concentration 0–50 μM. The detection limit of probe **1** was found to be 0.3 ppb. The authors also utilized probe **1** for the quantitative detection of palladium in real water samples using an indicator paper. Moreover, confocal microscopy experiments revealed that this ratiometric cell permeable fluorescent probe **1** could image palladium in live HeLa cells.

Koide's group developed the allylated 2′,7′-dichlorofluorescein derivative **2** to measure palladium contamination in laboratory chemicals.[28] Different chemical analytes (metal halides and metal oxides) were added to a mixture of allyl ether **2**, $NaBH_4$, and TFP (tri(2-furyl)phosphine) in DMSO/1.23 M phosphate buffer (pH = 7; 1 : 9 v/v) solution at a 0.5 mg mL^{-1} concentration. The resulting mixture was heated at 45 °C for 80 min. The same reaction was studied under same reaction conditions at various concentrations of palladium, *i.e.*, 0.1, 0.2, and 0.4 ppb. Exposure to either direct Pd(0) or palladium with different oxidation states in the presence of reducing agents converted the nonfluorescent fluorescein moiety to the highly fluorescent Pittsburgh Green derivative by cleaving the allylic ether bond (Fig. 2). Investigation showed that the fluorescence intensity showed a good linear relationship with the palladium concentration. The measured fluorescence intensities obtained

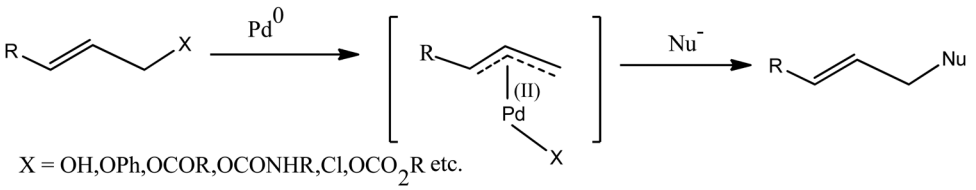

Scheme 2 Mechanism of Pd(0)-mediated cleavage of allyl ethers.

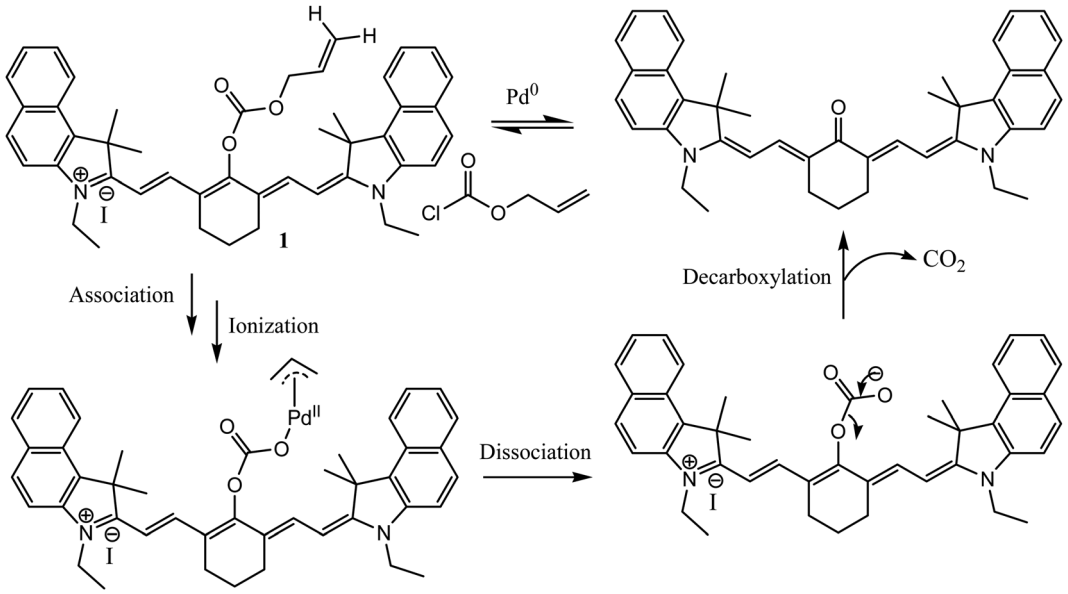

Fig. 1 Palladium-assisted (Pd^0) Tsuji–Trost allylic cleavage reaction of **1**.

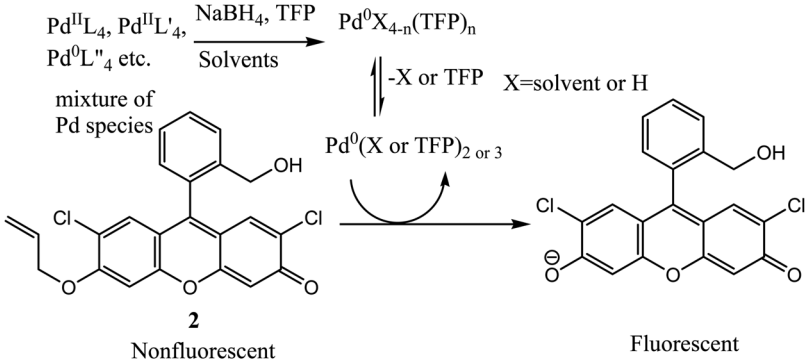

Fig. 2 Sensing strategy of the palladium-induced Tsuji–Trost reaction.

from the reaction with different chemical analytes were compared with the standard curve generated from the reaction with different concentration of palladium. From the compared data, the amount of palladium contamination was found in the palladium-contaminated chemical reagents. The chemodosimeter was also used as a quality control reactor using different reaction flasks to identify the highest palladium-contamination in the laboratory.

2.2. Suzuki–Miyaura coupling

Suzuki coupling or Suzuki–Miyaura coupling is the Pd-catalyzed cross-coupling reaction between organo-boron reagents and organo-halides (or triflates) in the presence of a mild base. This reaction can be used for generating a new C–C bond. This reaction was discovered by Akira Suzuki and Norio Miyaura in 1979.[29] The general catalytic cycle of Suzuki–Miyaura coupling includes three steps: (i) oxidative addition of the Pd(0) ligand [$L_nPd^{(0)}$] to alkyl, aryl, or vinyl halides to form the intermediate complex $L_nPd^{(II)}(R^2)X$ (R^2 = alkyl, aryl, or vinyl); (ii) metathesis involves the exchange of anion of the base (^-OR) with the anion (X^-) attached to the palladium intermediate species to generate $L_nPd^{(II)}(R^2)OR$; (iii) transmetallation between negatively charged base-activated boronate complex $[R^1B(R)_2(OR)]^-$ with the $L_nPd^{(II)}(R^2)OR$ complex to generate $L_nPd^{(II)}(R^2)(R^1)$; and (iv) Reductive elimination to give the final coupled product (R^1–R^2) and regenerating original palladium(0) species (Scheme 3).[30]

The Suzuki–Miyaura coupling reaction can be used to design functional polymers. Using this reaction, conjugated polymer-based fluorescent sensors can be synthesized. The sensors include (i) pyridine-based conjugated polymer chemosensors; (ii) imidazole-based conjugated polymer chemosensors; and (iii) Fused N-heterocycles-based conjugated polymer chemosensors.[31–33]

In 2011, Bradley designed probe **3** based on Pd(0)-catalyzed Suzuki–Miyaura cross coupling to transform the nonfluorescent aryl triflate moiety into highly fluorescent anthofluorescein derivative.[35] Cross coupling between two components caused extended conjugated moiety through the opening of the lactone

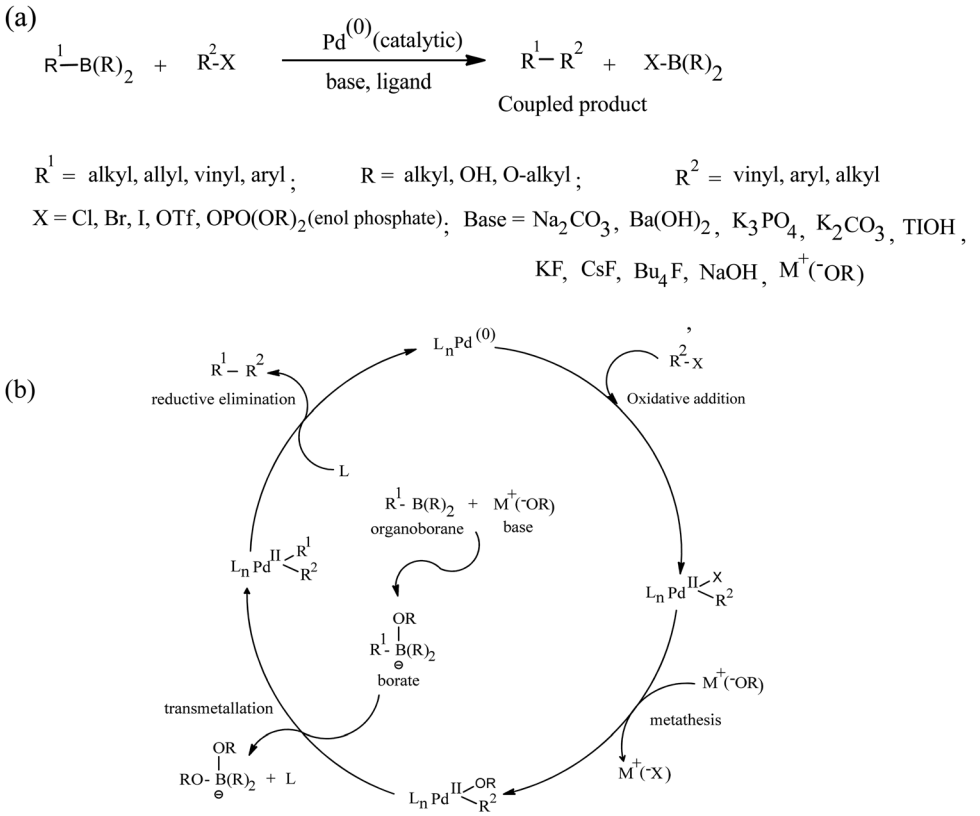

Scheme 3 (a) Plausible mechanism of Suzuki–Miyaura coupling. (b) Catalytic cycle of Suzuki–Miyaura coupling.[34]

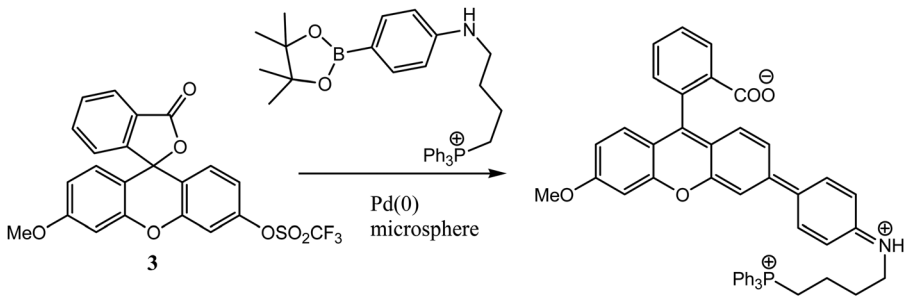

Fig. 3 Chemical structure of probe **3** and its chemodosimetric reaction.

ring. Using mitochondria targeting triphenylphosphonium moiety, they applied this probe **3** to localize Pd(0) in the mitochondria within the HeLa cells. The authors at first incubated the fluorescent-labelled Pd(0) microspheres within the HeLa cells before the injection of probe **3** and Mito Tracker. After incubation for 48 h, the cellular fluorescence images were taken by confocal microscopy. The confocal microscopy images showed the co-localization of the highly fluorescent dye and the Mito Tracker, which indicated Pd(0)-mediated intracellular aryl–aryl bond formation. The Pd(0) microspheres identified in the cytoplasm proved its potential ability to penetrate the cell membrane and remain intact inside the cytoplasm for several days. This was probably the first work where heterogeneous Pd(0) was used as a catalyst for labelling intracellular studies. This type of reaction will inspire researchers to develop the conjugated fluorescent molecules with the targeting moieties and practically use it in live cell imaging in pharmacology (intracellular formation of pro-drug-activated hydrophilic molecules) and medicine (systemic administration of locally-activated pro-drug molecules) purposes in the future (Fig. 3).

2.3. Claisen rearrangement

Allyl aryl and vinyl ethers undergo thermal intramolecular [3,3] sigmatropic rearrangement reaction to generate allyl phenols and unsaturated γ–δ carbonyl compounds, which is called the Claisen rearrangement (Scheme 4) and was named after the German scientist Rainer Ludwig Claisen, who was the pioneer of the above rearrangement reaction. The rearrangement reaction

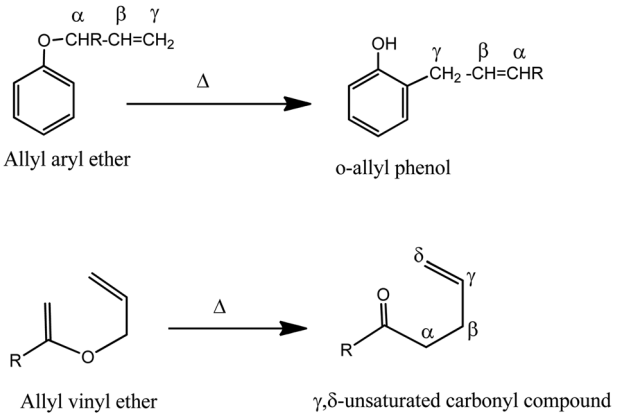

Scheme 4 Plausible mechanism of Claisen rearrangement.

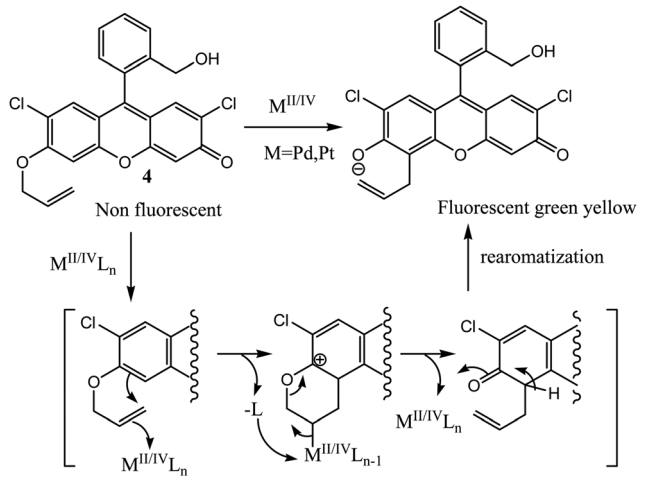

Fig. 4 Plausible catalytic Claisen rearrangement mechanism for the detection of Pd(II) and Pt(IV) using probe **4**.

passes through the formation of the six-membered cyclic transition state. Thus, through this rearrangement reaction, the allyl group of the allyl aryl ether moiety migrates to the *ortho* position of the benzene ring to generate the *o*-allyl phenol. This is a synthetic route to convert the allyl aryl ether molecule to its corresponding *o*-allyl phenol derivative.[36]

Garner *et al.* reported a metal-catalyzed aromatic Claisen rearrangement-based fluorescent probe **4** for the detection of Pd(II) and Pt(IV) species.[37] After 4 h, the rearrangement took place at 50 °C in 1 : 4 DMSO/pH 10 buffer solution only in the presence of the Pd(II) and Pt(IV) species and was not interfered by other metal species including Pd(0) under the same conditions. To measure the sensitivity of the probe, the authors also did an experiment using $PdCl_2$ under suitable detection conditions (1 : 1 DMSO/pH 10 buffer, and after 24 h). Investigation showed that with an increase in the incubation time, the intensity of the fluorescence signal also increased. The fluorescence intensity was correlated to the Pd(II) concentration in the range of 0.5–50 μM (50 ppb–5 ppm). From the above experiment, the calculated detection limit of probe **4** for Pd(II) was found to be 3.9 μM (390 ppb). They also applied probe **4** to detect Pt(IV) contamination in Pt(IV) contaminated water and to monitor the progress of the electrochemical reduction of Pt(IV) to Pt(0) in water. The detection limit of probe **4** for Pt(IV) was calculated to be 0.54 nM (0.11 ppb) (Fig. 4).

2.4. Benzil-cyanide reaction

Sessler and his coworkers first introduced the idea of the benzil-cyanide reaction for designing fluorescent chemosensors for cyanide (Scheme 5).[38] They first reported[39] probe **5** that underwent benzil rearrangement in an aprotic solvent and in the presence of TBACN (tetra butyl ammoniumcyanide) to produce cyanobenzoyl benzoate. But due to a lack of solubility in MeOH of probe **5**, no benzil-cyanide reaction-mediated bond cleavage took place and no detectable color change was observed. To overcome this problem, the authors designed an extended π-conjugated benzil probe **6**, which was soluble in MeOH. They utilized probe **6** with extended conjugation for the selective detection of cyanide in methanol–water (80 : 20) solvent system. Upon treatment with cyanide and base (10 μM, 1 N aqueous NaOH) to probe **6**, the peak centered at 410 nm displayed a large bathochromic shift near about 43 nm, accompanied by a naked eye color change from pale yellow to colorless. The color change was observed due to the addition of cyanide in aqueous methanol to probe **6**-triggered benzil-cyanide reaction-mediated bond cleavage, which caused a change in the π-conjugation. The sensing mechanism was monitored by LC-MS analysis. Moreover, the addition of cyanide and base to aqueous methanol in probe **6** resulted in a large fluorescence enhancement within 1 h. The limit of detection (LOD) of probe **6** was less than 1.7 μM (Fig. 5).

2.5. Intramolecular crossed-benzoin reaction

Suzuki and his coworkers first reported intramolecular crossed benzoin reaction using the thiazolium precatalyst.[40] It is generally an extension of the simple benzoin condensation reaction (condensation between two aldehydes in the presence of cyanide to give α-hydroxy ketones or benzoins). But here, instead of using two simple aldehydes, intramolecular cross condensation reaction occurs between aldehyde and ketone to give the six-membered cyclic acyloins. This reaction can be used in cyclic ring formation.

Kim and coworkers designed probe **7** based on intramolecular crossed-benzoin condensation for the selective sensing of cyanide in aqueous environments.[41] On the addition of KCN to the PBS buffer, the absorption intensity at 565 nm increased 20-fold, accompanied by a change in the color of the solution from pale orange to deep pink. With an increase in the CN^- concentration, the fluorescence intensity at λ_{em} = 595 nm gradually increased over the range of 0–3 equiv. The significant turn-on fluorescence response was caused by intramolecular crossed benzoin reactions, which released highly fluorescent resorufin when cyanide was added to probe **7**. Probe **7** was very sensitive to CN^- and showed rapid fluorescence response within 10 s. This sensing mechanism was confirmed by ^1H NMR titration and mass spectroscopy. The detection limit of the probe was as low as 4 nM. The authors also showed the selectivity of the probe using test stripes coated with

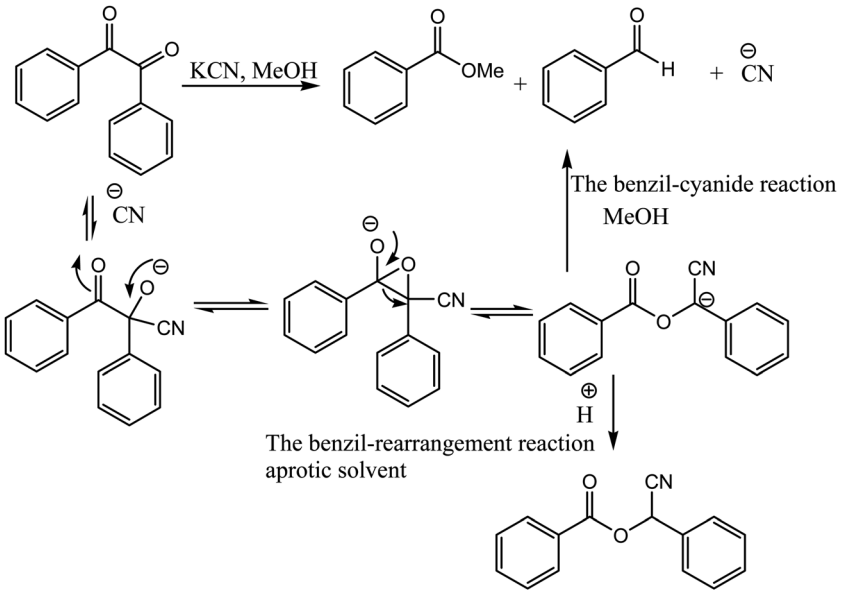

Scheme 5 Proposed reaction mechanisms of the benzil-rearrangement and benzil-cyanide reaction.

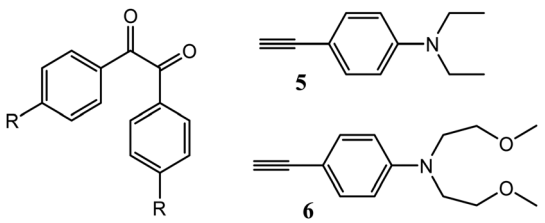

Fig. 5 Structure of probes **5** and **6**.

probe 7. After the addition of various anions of potassium salts, *i.e.*, CN^-, F^-, Cl^-, Br^-, I^-, $CH_3CO_2^-$, HPO_4^{2-}, HCO_3^-, NO_3^-, ClO_4^-, and SCN^- and some neutral species, *i.e.*, Cys, Hcy, and GSH, only a significant color change to pink and fluorescence change were observed in the case of cyanide, proving the probe's potential use for the sensing of potassium cyanide in the presence of other analytes. They also utilized the probe for the bioimaging of KCN in live HeLa cells and blood serum (Fig. 6).

2.6. Michael addition

Michael addition is base-catalyzed 1,4 conjugate addition of a nucleophile to the double bond of an α,β-unsaturated carbonyl compound to give 1,4-Michael adduct (Scheme 6). This reaction was named after Arthur Michael, who discovered the above reaction in 1887. This reaction has practical utility to generate new C–C bonds.[42]

2.6.1. Cyanide chemodosimeters. Cyanide, being a good nucleophile, can attack the α,β-unsaturated probe through Michael addition. Park *et al.* reported an α,β-unsaturated carbonyl moiety-based probe **8** for the recognition of cyanide.[43] Upon the addition of CN^- in acetonitrile, the absorption maxima at 430 nm ($\varepsilon = 3.9 \times 10^4\ M^{-1}\ cm^{-1}$) decreased and a new peak at 260 nm ($\varepsilon = 2.8 \times 10^4\ M^{-1}\ cm^{-1}$) appeared, accompanied by a change in the color of the solution from yellow to colorless. An isosbestic point observed at 272 nm clearly indicated the formation of a new species. Due to photo-induced electron transfer from diethylamine phenyl to hydrogen-bonded carbonyl group, the quenching of fluorescence of probe **8** was observed. But upon the addition of cyanide to probe **8** in CH_3CN, a strong turn-on blue fluorescence was observed at 469 nm. Due to effective intramolecular hydrogen bonding of the *o*-hydroxyl group to the α,β-unsaturated carbonyl group, the double bond was sufficiently activated to act as a Michael acceptor to facilitate the nucleophilic attack of cyanide, resulting in an enol intermediate, which, *via* tautomerization, generated a stable keto form to furnish the fluorescent phenolate and, as a result, a 1300-fold fluorescence intensity enhancement was observed. The authors also showed that the hydrogen bonding effect was important as the hydrogen-bonded enone intermediate behaved as a sufficiently-strong electrophile to induce the nucleophilic attack of cyanide to show naked-eye fluorescence turn on signal. They also reported that without hydrogen bonding, no such naked eye change was observed. The reaction pathway was monitored by ^1H NMR spectroscopy. Job's plot showed that the stoichiometry between probe **8** and CN^- was 1 : 1. The detection limit of probe **8** for cyanide detection was found to be 1.7 μM. The time-dependent fluorescence study showed that the reaction followed pseudo first order kinetics and the rate constant was found to be $8.2 \times 10^{-5}\ s^{-1}$. The authors also applied probe **8** for the detection of cyanide in drinking water and also for the detection of lethal levels of cyanide in fire victims (Fig. 7).

Sun *et al.* designed and synthesized a 3-amido coumarin-based fluorescent probe **9** for the colorimetric detection of cyanide.[44] Upon the addition of CN^- to probe **9**, the intense absorption band at 332 nm gradually decreased and finally vanished but the intense absorption band at 301 nm gradually increased with the formation of an isosbestic point at 307 nm.

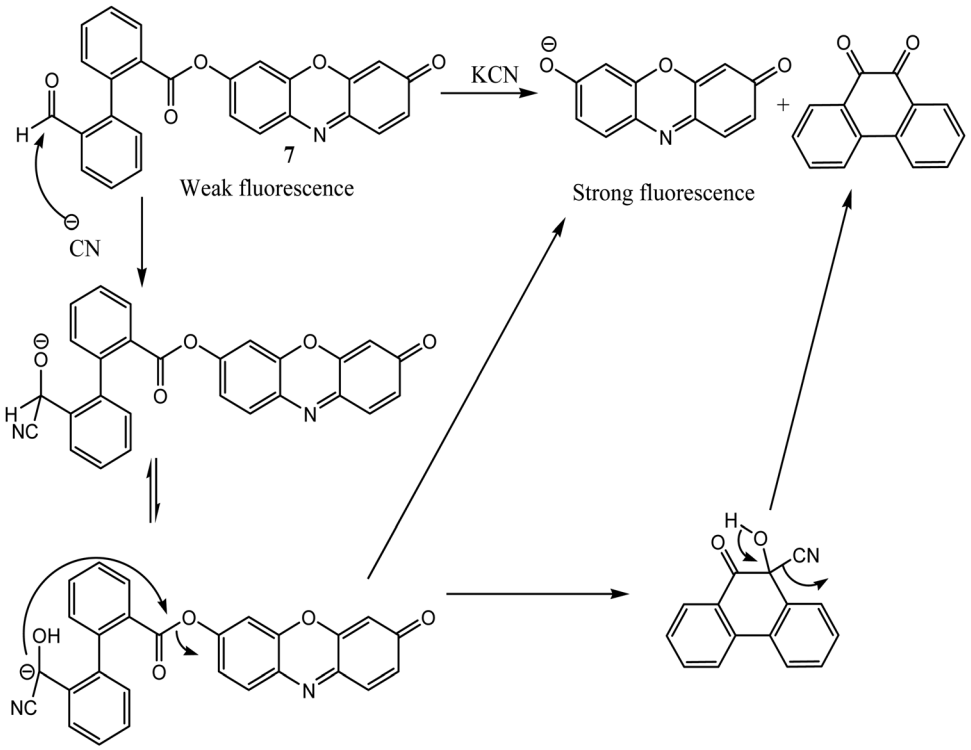

Fig. 6 KCN-assisted intramolecular crossed benzoin reaction of probe **7**.

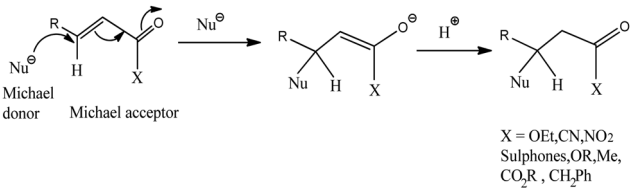

Scheme 6 Plausible mechanism of Michael addition.

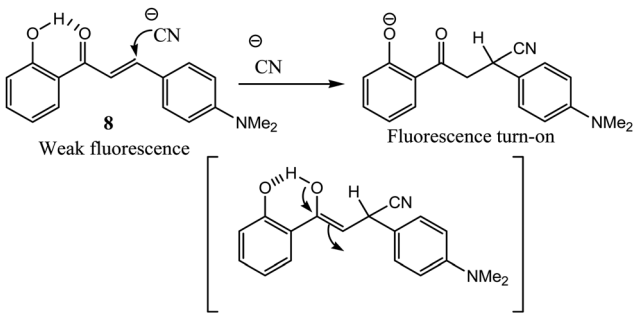

Fig. 7 CN^- induced Michael addition reaction of probe **8**.

Probe **9** exhibited very weak fluorescence with low quantum yield (Φ = 0.002) and after the addition of cyanide, no change in fluorescence was observed. But compound **10** exhibited strong fluorescence with a quantum yield of Φ = 0.11. Upon the addition of CN^-, the fluorescence intensity at 403 nm gradually decreased, resulting in a blue shift of about 10 nm. The authors stated that the reason behind this is the change in the C–N bond length from probe **10** to its cyanide binding adduct, which remains unchanged in the case of compound **10** and its adduct. The above results proved the reaction pathway, *i.e.*, the reaction occurred through intramolecular cyclization between the cyano and amido groups, followed by the Michael addition of cyanide at the 4-position of coumarin. Probe **9** was very sensitive toward CN^- and showed rapid response within 10 s. From Job's diagram, it was obtained that CN^- showed 1 : 1 reaction stoichiometry for both probes **9** and **10**. The reaction intermediates were characterized by ^{1}H NMR and mass spectroscopy. From X-ray diffraction study, they also confirmed that the attack of cyanide took place at the 4-position of coumarin (Fig. 8).

Lee *et al.* introduced enone-functionalized benzochromene probe **11** as a ratiometric fluorescent chemosensor for the detection of cyanide in aqueous buffer solution.[45] The sensing of cyanide occurs through Michael addition. Upon the addition of CN^-, the absorption band at 388 nm decreased and a new band appeared at 297 nm, accompanied by a naked eye color change from light yellow to colorless. Two clear isosbestic points at 315 nm and 418 nm clearly indicated that new species were being formed. Moreover, the fluorescence emission band was blue shifted from 518 nm to 350 nm upon the addition of CN^- and the fluorescence color of the solution changed from strong green to weak blue. The Michael addition of CN^- to probe **11** induced lactone ring-opening to give a keto–enol-tautomerized intermediate, which subsequently underwent the [1,3]-sigmatropic rearrangement reaction to give a free phenol product, which was responsible for the above changes in the

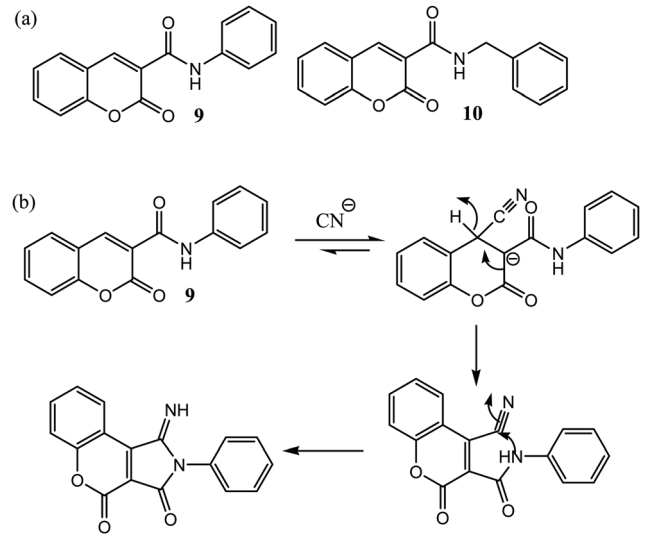

Fig. 8 (a) Chemical structures of probe **9** and **10**. (b) CN^--assisted Michael addition reaction of probe **9**.

optical and spectroscopic properties upon the addition of CN^- to probe **11**. The sensing mechanism was confirmed by ^1H NMR and mass spectroscopy. The fluorescence intensity ratio $F_{518\,nm}/F_{350\,nm}$ of probe **11** showed a ratiometric fluorescence response toward cyanide. The detection limit of probe **11** for cyanide detection was found to be 5.3 μM. The kinetic study showed that the reaction followed second order kinetics and the rate constant was found to be $k = 3.8 \times 10^{-3}\ M^{-1}\ s^{-1}$. The authors further demonstrated that probe **11** could act as a ratiometric fluorescent chemodosimeter for the detection of toxic cyanide in aqueous solutions (Fig. 9).

2.6.2. Biothiol chemodosimeters. Yang *et al.* reported a semi-napthofluorescein-based probe **12** for sensing biothiols (cysteine) based on 1,4-conjugate additions to α–β unsaturated carbonyl compounds.[46] Upon the addition of cysteine, a naked eye color change was observed from colorless to pink. The emission intensity band at 621 nm gradually increased upon the gradual addition of cysteine. The color change was due to 1,4-conjugate additions of cysteine to the double bond to give the addition product $\mathbf{I_1}$, which underwent intramolecular cyclization to a stable 7-membered intermediate $\mathbf{I_2}$, releasing semi-napthofluorescein (**12a**). The investigation showed that the reaction completed within 20 min after the addition of cysteine, and the detection limit of probe **12** was found to be 0.2 μM. The authors further applied chemodosimeter **12** for the selective detection of cysteine in biological samples (Fig. 10).

Zhang *et al.* reported an imidazole core unit based on luminescent aggregate **13** with a hydroxynapthalene head group and a benzyl tail unit.[47] With the addition of cysteine in PBS buffer (20 mM, pH 7.2) solution of probe **13**, the emission intensity of the keto-form increased gradually, whereas the intensity of the enol-form increased at first, then gradually decreased. The first increase in the emission intensity of the enol form was attributed to the conjugate addition of cysteine to the double bond, inhibiting photoinduced electron transfer process and then, due to the formation of the lactam ring, induced product **13a** to exhibit an ESIPT (excited-state intramolecular proton transfer) process *via* intramolecular proton transfer, which was responsible for the increase in keto emission. Moreover, upon the addition of cysteine to the probe solution, a weak emission peak at 425 nm, corresponding to the enol tautomer and a strong emission peak at 553 nm, corresponding to keto tautomer, were observed. To show the selectivity of the probe toward cysteine, the authors also compared the intensity of the enol emission peak in the presence of cysteine with other structurally similar biothiols, *i.e.*, Hcy and GSH. It was observed that the intensity of enol emission peak after addition of Hcy and GSH was strong compared to Cys, which indicated the removal of these groups, *i.e.*, Hcy and GSH, did not easily take place after conjugation with probe **13**. Also, the keto–enol ratio for Cys was 12 with yellowish-green emission, whereas for Hcy and GSH, the ratio was 2 with blue emission, indicating that probe **13** was highly selective toward cysteine recognition. The authors also investigated the fact that the ratio of the keto/enol tautomer of product **13a** varied with the solvent polarity. Depending on the solvent polarity, different emission colors were observed in different solvent media due to the varying content of the keto/enol tautomer. The weak enol form emission peak centered at 415 nm showed a remarkable red shift at ~553 nm in polar solvent (DMF) and protic solvent (EtOH), accompanied by yellow and green emission, respectively. In nonpolar solvents, *i.e.*, in benzene and DCM, the emission peak was observed at 600 nm with orange yellow emission and in cyclohexane, the emission peak was observed at 610 nm with red emission. The large Stokes shift was due to the transformation of the enol form to the keto form *via* proton transfer of imidazole NH

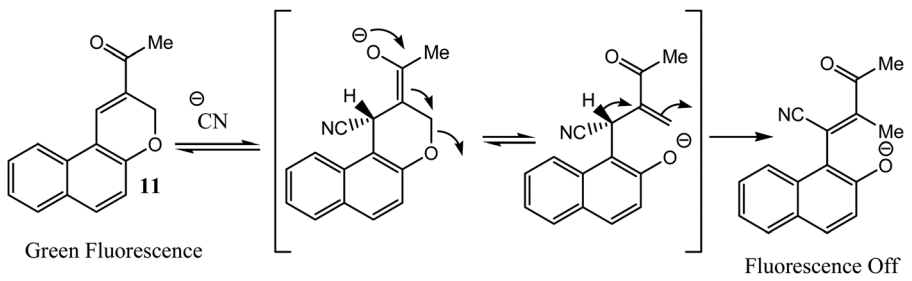

Fig. 9 CN^--assisted Michael addition reaction of probe **11**.

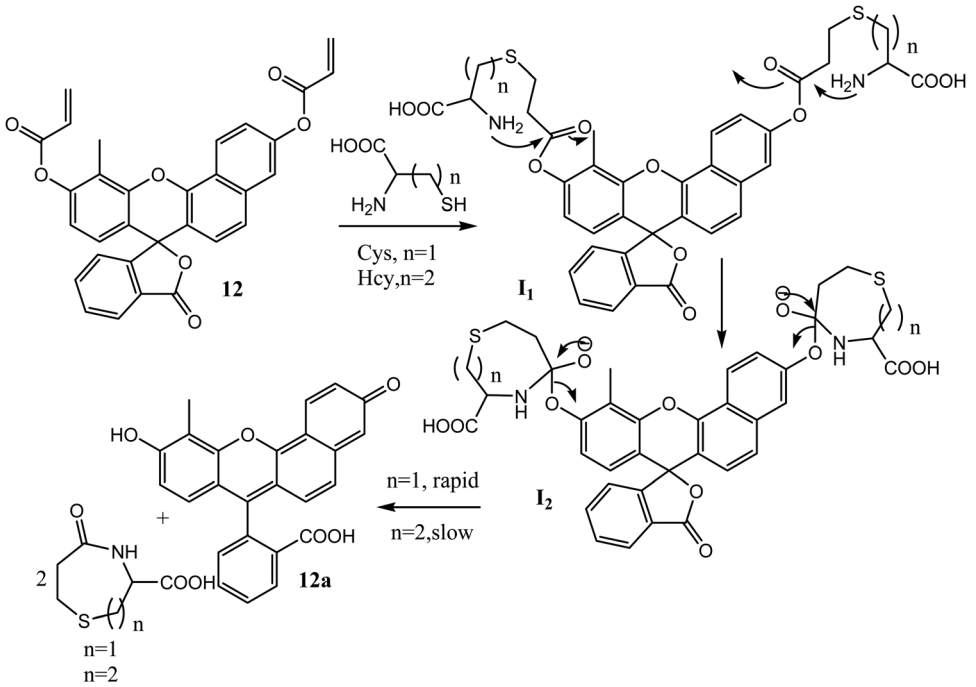

Fig. 10 Plausible cysteine sensing mechanism of probe **12**.

through ESIPT, resulting in an increase in the conjugated chain length, which indicated that product **13a** mainly existed in the keto form in the nonpolar solvent. Moreover, the normal keto form emission of product **13a** was observed at (> 540 nm) with large Stokes shifts in strong polar and protic solvents but displayed different bathochromic shifts in different solvents, *i.e.*, 553 nm in DMF and 610 nm in cyclohexane, depending on the extent of stabilization of the n–π* transition of the keto form in different solvent systems. The authors also reported an emission intensity change for product **13a** in DMF with varying concentrations. At very low concentrations, *i.e.*, 2.5 μM, a weak emission peak was observed mainly at 480 nm due to the interaction of product **13a** with the solvent DMF. But with increasing concentration, two new shoulders at 415 nm and 565 nm appeared, corresponding to the enol and keto tautomer, respectively. The investigation showed that with an increase in the concentration from 2.5 μM to 100 μM, the enol emission intensity peak gradually disappeared and a keto form emission intensity peak existed mainly at 565 nm, accompanied by a change in the color of the solution from blue, yellow, to bright yellow. The main existence of keto form emission was due to increased planarity and rigidity in the keto form, which restricted the molecular motion by J-aggregation. The authors also studied the effect of water concentration on the emission of product **13a**. Investigation showed that for up to 80% water content, the enol form predominated due to hydrogen bonding with water, which inhibited intramolecular proton transfer through the ESIPT process to give the keto form. But above that, for up to 100% water content, mainly the keto form predominated due to the aggregation of product **13a** into nanoparticles. This was also clear from the change in the color of the solution from yellowish green (0%), yellow (60%), to green (100%). The emission intensity of the keto form increased linearly with cysteine concentration in the range from 0 to 30 μM. The detection limit of the probe for cysteine detection was found to be 0.21 μM (Fig. 11).

Manna *et al.* reported two intramolecular charge transfer (ICT)-based fluorescent probes, **14** and **15**, based on the acrylate group as the cysteine recognition unit.[48] With the addition of cysteine to probe **14** in aqueous DMSO (DMSO : H_2O = 7 : 3 v/v, 10 mM HEPES buffer, pH = 7.4), the absorption peak at 272 nm gradually decreased and a new peak appeared at 410 nm with an isosbestic point at 347 nm. It was also observed that the absorption maxima showed a red shift of about 138 nm upon the addition of cysteine and the color of the solution changed from colorless to yellow. Upon the addition of cysteine to probe **14**, a nearly 992-fold enhancement in the fluorescence intensity was observed at 506 nm. The removal of the acrylate moiety upon the addition of cysteine generated a phenoxide moiety, which facilitated the ICT process and the fluorescence color of the solution changed from colorless to intense green. But no such significant fluorescence enhancement was observed for probe **15**. This was because in the presence of cysteine, the cleavage of the acrylate moiety occurred at 7-positions in probe **14**, which resulted in an enhancement in the ICT process but in the case of probe **15**, the cleavage occurred at 2-positions under identical conditions for which no such ICT process was observed. Moreover, the fluorescence intensity at 506 nm of probe **14** varied with cysteine over a wide range of concentrations of 0–1.25 equiv. The detection limit of probe **14** was found to be 47 ppb. To justify the selectivity of the probe, the authors also did the experiments in the presence of biothiols (Cys, Hcy, GSH) and other amino

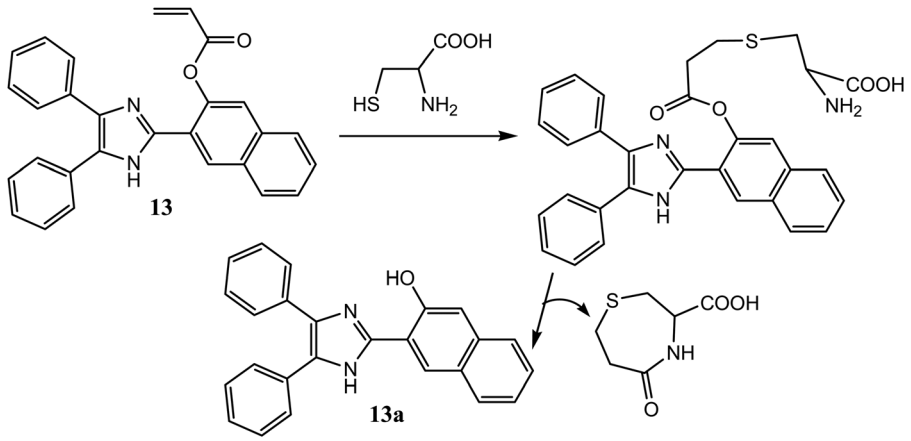

Fig. 11 Structure of probe **13** and its sensing mechanism with cysteine.

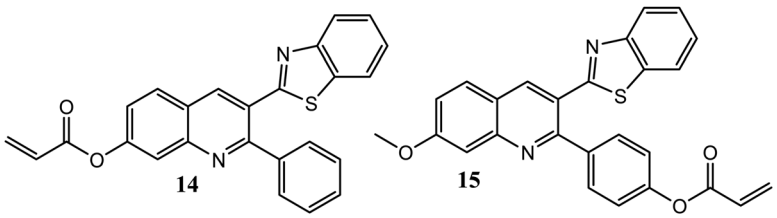

Fig. 12 Structures of probe **14** and **15**.

acids (Ala, Glu, Arg, Lys, Asp, Gly, Leu, Tyr, His, Trp, Ile, Thr, Phe, Pro, Met, and Val). Investigation showed that the naked eye color and fluorescence change only in the case of cysteine. The authors explained the fact by considering seven-membered ring formations through Michael addition and intramolecular cyclization in the presence of Cys, whereas in the presence of Hcy, eight-membered ring formations took place. As seven-membered ring formation was entropically more favorable compared to eight-membered ring formation, probe **14** showed selective response toward Cys in the presence of other structurally similar biothiols, *i.e.*, Hcy and GSH. The reaction mechanism was also proved by ^{1}H NMR and mass spectroscopy. Time-dependent fluorescence spectroscopy showed that the reaction completed within 12 min after the addition of Cys. The authors also applied probe **14** for cysteine recognition in osteosarcoma (MG-63) live cells (Fig. 12).

Feng and coworkers developed the acrylate-conjugated benzopyran-based NIR fluorescent probe **16** for the recognition of biothiols (cysteine, Hcy, and GSH).[49] Upon the gradual addition of cysteine to the DMSO–PBS buffer solution (10 mM, pH = 7.4, 1 : 1, v/v), the absorption maxima showed a red shift of about 160 nm (395 nm to 555 nm) and a naked eye color change was observed from light yellow to pink. In addition, after treatment with cysteine, the NIR fluorescence emission intensity band at 706 nm was also enhanced. The fluorescence enhancement was observed due to cysteine-triggered acryloyl moiety cleavage of probe **16**, releasing a highly NIR fluorescent molecule. The fluorescence intensity ratio of probe **16** varied linearly with cysteine concentration in the range of 0–10 μM. The detection limit of probe **16** for cysteine detection was 81 nM. To justify the selectivity of the probe, the authors also carried out an experiment in the presence of biothiols and other amino acids. Among these species, significant color change was observed only in the case of biothiols. From the above experiment, it was clear that the probe was highly selective toward biothiols (Cys and Hcy). To compare the response difference between biothiols and the rate of reaction, the authors also studied time-dependent fluorescence studies. Investigation showed that the order of the rate of reaction of biothiols is Cys > Hcy > GSH. The reaction followed pseudo-first order kinetics and the rate constant for cysteine recognition was found to be $k_{obs} = 0.167\ min^{-1}$ ($t_{1/2} = 4.15$ min), which indicated that the reaction between probe **16** and cysteine was very fast. The results clearly indicated that probe **16** could be used as an NIR fluorescent turn-on sensor to detect cysteine rapidly in aqueous solution. The product was isolated and characterized by ^{1}H NMR and mass spectroscopy. They also applied this probe for the bioimaging of cysteine inside the HeLa cells (Fig. 13).

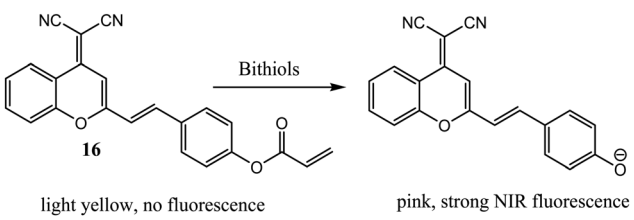

Fig. 13 Chemodosimetric reaction of probe **16** with biothiols.

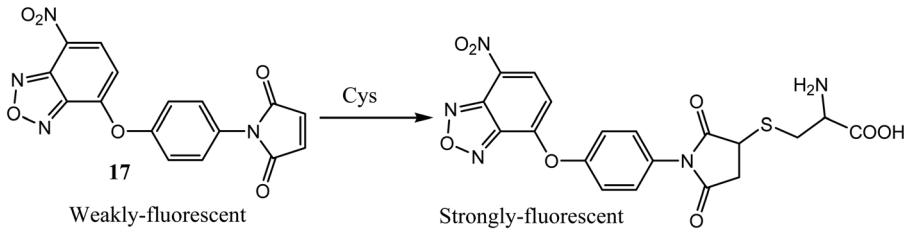

Fig. 14 Chemodosimetric reaction of probe **17** with cysteine.

The Michael addition reaction was also widely used for cysteine[50–56] recognition based on the bioconjugation of thiol-containing molecules to maleimide receptors.[57]

Shen *et al.* designed benzoxadiazole (NBD)-linked maleimide-based receptor **17** for thiol recognition based on Michael addition.[58] Upon the gradual addition of cysteine to probe **17**, the absorption maxima at 380 nm gradually decreased with the simultaneous appearance of a new absorption maxima at 490 nm, *i.e.*, the absorption maxima displayed a red shift (110 nm) from 380 nm to 490 nm with a naked eye color change of the solution from colorless to yellow. After treatment with cysteine, a significant enhancement in the emission intensity band at 554 nm was observed with a fluorescence color change from dark to green. The significant enhancement of emission intensity was due to the nucleophilic attack of the sulphur anion of cysteine on the electrophilic maleimide moiety, which caused significant charge transfer from maleimide to NBD. Furthermore, probe **17** showed a linear relationship with cysteine over a range of concentration of 0–70 μM. From Job's plot, it was obtained that cysteine showed 1 : 1 reaction stoichiometry toward probe **17**. The detection limit of probe **17** for cysteine recognition was found to be 1.2×10^{-7} M. The authors also studied the pH effect of the probe. The investigation showed that the probe displayed strong fluorescence only at pH 7.0, *i.e.*, the biological pH region. They also applied this probe **17** for the detection of thiols in HeLa cells (Fig. 14).

Nagano and coworkers designed the BODIPY-based probe **18** for thiol (*N*-acetyl cysteine) recognition.[59] They also investigated the fact that the position of the maleimide substituent to the BODIPY core played a key role in effective fluorescence quenching. It was observed that effective fluorescence quenching through donor-excited photoinduced electron transfer (d-PET) happened in the case of the *ortho*-substituted maleimide derivative of BODIPY compared to its *meta* and *para* substitution. The observed fact was due to the minimized distance between the electron donor and the electron acceptor in the PET process in the case of *ortho*-substitution compared to the others. Thus, the *ortho*-substituted maleimide derivative of BODIPY, which quenched fluorescence through PET, showed a strong turn-on fluorescence response toward thiols. Upon the addition of thiols, near about 350-fold enhancement of fluorescence emission intensity was observed with an emission color change of the solution from colorless to bright green and the fluorescence quantum yield changed from $\Phi = 0.002$ to $\Phi = 0.73$. The large increase in the fluorescence quantum yield was observed due to the inhibition of the d-PET process from BODIPY to maleimide

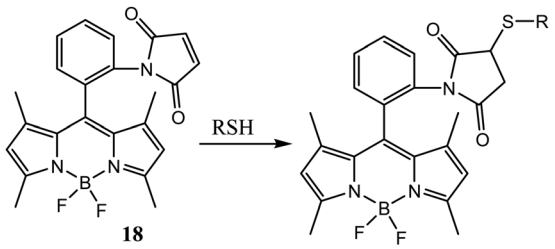

Fig. 15 Chemodosimetric reaction of probe **18** with biothiols.

upon the addition of thiols. They also applied this probe **18** for monitoring the level of bovine serum albumin (Fig. 15).

Yi *et al.* also introduced a coumarin-based fluorescent probe **19** for thiol recognition.[60] The probe was highly selective toward thiols (GSH, Cys, β-mercaptoethanol) in the presence of other amino acids. Upon the addition of thiols to probe **19**, immediate naked eye blue green fluorescence emission was observed. The significant turn-on fluorescence response was due to the Michael conjugate addition of the thiols to the *cis* double bond of probe **19**, causing significant quenching of the PET process. Probe **19** was also used for monitoring the level of GSH inside the cells. Probe **19** showed very weak fluorescence intensity ($\Phi = 0.001$) due to the effective PET process operating through the intramolecular double bond. But after the addition of GSH to probe **19**, a large increase in the fluorescence quantum yield ($\Phi = 0.47$) was observed. Upon addition of GSH to probe **19**, the increase in the fluorescence quantum yield was more than 470-fold due to the inhibition of the PET process, which was operative through the intramolecular double bond. Moreover, the fluorescence intensity of probe **19** was linearly proportional to the GSH concentration in the range of 0–100 nM. The detection limit of probe **19** for GSH detection was found to be at least less than 0.5 nM. Probe **19** was also used to detect the quantity of GSH inside the cells based on an enzymatic assay for glutathione reductase. Glutathione reductase (GR) is an enzyme that catalyzes the conversion of GSSG to GSH using NADPH. Probe **19** gave a strong turn-on fluorescence response with a rise in the amount of glutathione reductase when the initial concentration of the substrate and NADPH was the same. The maximum reaction rate was linearly proportional to glutathione reductase concentration in the range between 0.1 and 0.75 mU mL^{-1} for two different substrate concentrations, from which unknown concentration of glutathione reductase was calculated. The probe was also sensitive to β-mercaptoethanol

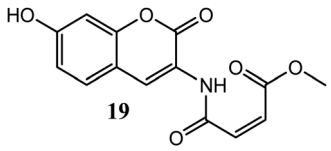

Fig. 16 Structure of probe **19**.

and cysteine. The time-dependent fluorescence response study showed that the reaction between probe **19** and β-mercaptoethanol followed the pseudo-first order kinetics. The observed rate constant (K_{obs}) between probe **19** and β-mercaptoethanol at pH 7.4 and 25 °C was found to be 2.3×10^2 s^{-1} ($t_{1/2}$ = 3 ms), which was 7.0×10^4 M^{-1} s^{-1} in the case of cysteine. The above data indicated the higher rate of reaction between probe **19** and cysteine, resulting in rapid fluorescence response within less than one min at room temperature. The authors further showed that when probe **19** was incubated with HEK-293 cells, a strong fluorescence response within 5 min was observed, proving its potential ability to monitor the level of the thiols inside the cells. Moreover, the high level of GSH inside the cells may cause different diseases. Hence, probe **19** could be used to control cytosolic GSH level inside the cells based on an enzymatic assay (Fig. 16).

2.7. Gabriel mechanism

Gabriel amine synthesis method[61] has been attractive nowadays for hydrazine recognition. This method involves two steps. The first step is the phthalimide anion being alkylated to form *N*-alkyl phthalimide, and then the *N*-alkyl phthalimide is cleaved by hydrazine to form the primary amine (Scheme 7). The above reaction was named after the German scientist Siegmund Gabriel in 1887 who invented it along with his partner James Dornbush.

Cui *et al.* displayed a 1,8-napthalimide fluorescent probe **20** for selective hydrazine recognition based on the Gabriel mechanism.[62] The treatment with hydrazine in H_2O/DMSO (4 : 6, v/v) solution triggered the deprotection of the phthalimide part, generating highly fluorescent amine and the absorption peak at 340 nm decreased with the simultaneous appearance of a new absorption peak at 440 nm with an isosbestic point at 380 nm. Upon this cleavage, the probe solution showed a naked eye color change from colorless to yellow. Moreover, the addition of N_2H_4 fluorescence intensity was enhanced by about 100-fold at 540 nm with the emission of strong yellow fluorescence. The fluorescence intensity at 540 nm displayed a good linear relationship with [N_2H_4] over

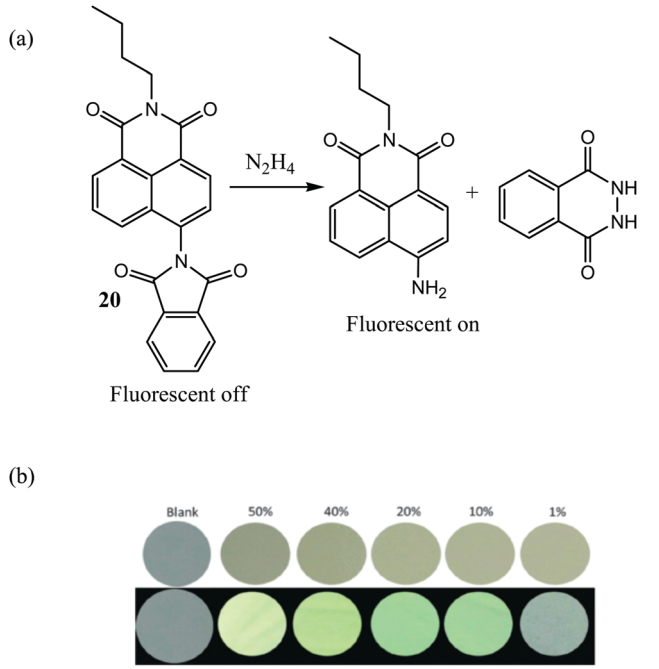

Fig. 17 (a) Chemodosimetric reaction of probe **20** with hydrazine; (b) visual and fluorescence color change of probe **20** (5.0 mM)-coated TLC plates + different concentrations of hydrazine in aqueous solution. Reproduced/adapted from ref. 62 with permission from The Royal Society of Chemistry.

a wide range of concentrations of 1–50 μM. The detection limit of probe **20** for gaseous N_2H_4 detection was found to be 111.7 mg m^{-3} and in solution phase detection, the detection limit of probe **20** was found to be 0.3 ppb. Time-dependent fluorescence response study showed that the reaction was completed within 100 s, indicating rapid response toward hydrazine. The authors also reported the fastest response of probe **20** compared to all other previously reported probes. Due to the presence of strong electron withdrawing 1,8-naphthalimide moiety, the nucleophilic substitution reaction was facilitated to occur at a faster rate compared to the others. Furthermore, utilizing the convenient test kits, this probe might be utilized for gaseous phase hydrazine detection. Finally, fluorescent imaging studies show that this probe **20** may be used to visualize hydrazine in HeLa cells (Fig. 17).

Mahapatra and coworkers reported a highly selective and sensitive benzothiadiazole-based fluorescent probe **21** for the detection of hydrazine.[63] With the addition of N_2H_4 to H_2O–DMSO (4 : 6 v/v, 10 mM HEPES buffer, pH 7.4) solution, two

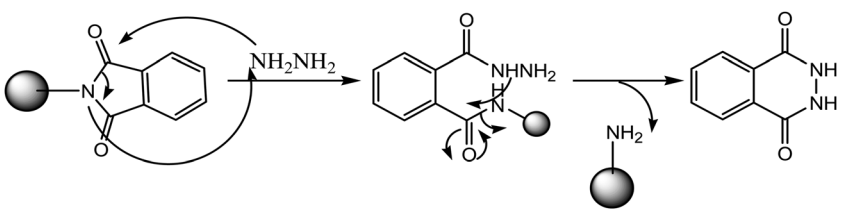

Scheme 7 Plausible mechanism of Gabriel amine synthesis.

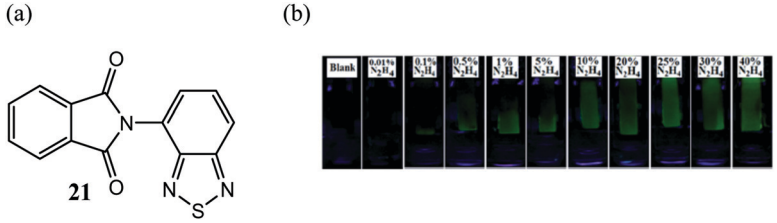

Fig. 18 (a) Structure of hydrazine sensing probe **21**. (b) Fluorescence color change of probe **21** coated TLC plates + different concentrations of hydrazine in aqueous solution. Reproduced/adapted from ref. 63 with permission from The Royal Society of Chemistry.

major absorption bands at 306 nm and 313 nm decreased with the sudden appearance of a new absorption band at 395 nm, and a naked eye color change was observed from colorless to yellow with the formation of a new isosbestic point at 362 nm. After treatment with hydrazine, a near 9.05-fold enhancement of fluorescence emission intensity was observed at 498 nm with an emission color change from colorless to bright green. The fluorescence intensities of probe **21** were linearly proportional to the $[N_2H_4]$ concentration in the range of 0.025–1.5 μM. Job's diagram proved that hydrazine showed 1 : 1 reaction stoichiometry of the probe. Time-dependent fluorescence study showed that after the addition of hydrazine, significant fluorescence enhancement was observed within 20 min. The detection limit of probe **21** was found to be 8.47×10^{-8} M (2.9 ppb). They also applied probe **21** for the detection of hydrazine in real water samples and for the bioimaging of hydrazine in live Vero 76 cells (Fig. 18).

Das and coworkers designed and synthesized a phenanthroline derivative-based fluorescent chemodosimeter **22** for the selective detection of hydrazine.[64] Probe **22** displayed an absorption maximum at 329 nm ($\varepsilon = 2.55 \times 10^{-4}$ L mol^{-1} cm^{-1}) by virtue of π–π* transition between the phenanthrene and benzimidazole moiety. However, upon the addition of N_2H_4 to the probe solution, no change in the absorption spectra was observed. Upon treatment with N_2H_4, the probe showed a 60-fold fluorescence enhancement value. The fluorescence intensity at 540 nm varied linearly with $[N_2H_4]$ concentration in the range from 0 to 30 μM. The detection limit of the probe was found to be 1.5 ppb. The time-dependent fluorescence response study showed that the reaction was completed within 40 min, and the rate constant (K) was found to be 2.76×10^{-4} s^{-1}. They also applied probe **22** for the quantification of the intracellular release of N_2H_4 in Hct 116 or HepG2 cells. Patients of tuberculosis consuming isoniazid drugs can suffer from liver toxicity, which is due to the metabolism of isoniazid. Aminoacylase-1 enzyme catalyzes the metabolism of isoniazid producing hydrazine. After the administration of probe **22**, significant fluorescence enhancement was observed in the presence of aminoacylase-1, which gave a measurement of liver toxicity through an enzymatic assay.

Zhao *et al.* reported a highly sensitive colorimetric and fluorometric probe **23** for hydrazine detection.[65] In HEPES buffer (pH 7.0, 20 mM) and DMSO (1/9, v/v) solution, probe **23** showed an absorption band at 365 nm. Upon exposure to hydrazine, the absorption at 365 nm gradually blue-shifted about 33 nm, accompanied by a change in the color of the solution from yellow to colorless. The isobestic point at 353 nm indicated the formation of new species. Hydrazine-induced cleavage caused an enhancement in the emission intensity of the solution with a change in the color of the solution from light yellow to strong greenish-yellow. The emission band centered at 475 nm was shifted to 512 nm. A time-dependent fluorescence response study showed a significant emission intensity change within 1 h after the addition of hydrazine. The detection limit of probe **23** was found to be 6.01 ppb. The authors also studied the pH effect of probe **23** in the presence of hydrazine. The investigation showed that with an increase in the pH, the fluorescence intensity gradually increased, reached a maximum only at pH 7.0, and then again gradually started to decrease at pH 9.0. The decrease in the fluorescence intensity with an increase in the pH was due to the decomposition of the amide moiety. The above results showed that probe **23** could be used for the practical use for biological and environmental purposes. The authors described test kit experiments for detecting hydrazine in vapor and aqueous phases. The probe was also utilized to detect hydrazine in tap water and river water samples. In addition, confocal microscopic imaging proved that the probes could be used for the detection of hydrazine in HeLa cells.

Wang and his coworkers reported a highly sensitive fluorometric probe **24** for hydrazine detection.[66] Upon the addition of hydrazine to PBS buffer solutions (pH 7.4, 10 mM, 30% CH_3CN) of probe **24**, the absorption band centered at 380 nm blue-shifted to 370 nm. Moreover, on exposure of the probe solution to hydrazine, the emission band showed a red-shift from 450 nm to 490 nm with an 84.7-fold enhancement of the fluorescence emission intensity and the fluorescence color of the solution changed from colorless to bright blue. The observed turn-on fluorescence emission intensity was due to the quenching of the PET process by virtue of demasking of the phthalimide group, which was operated in a free probe from the pyrazoline fluorophore to the phthalimide moiety. The fluorescence intensity at 490 nm varied linearly with $[N_2H_4]$ concentration in the range of 10–20 μM. The detection limit of the probe was found to be 1.99 ppb or 0.0622 μM. Probe **24** showed a response to hydrazine within 4 min. To justify the selectivity of probe **24**, the authors also studied fluorescence properties in the presence of various analytes, *i.e.*, cations (Fe^{3+}, Cd^{2+}, Cu^{2+}, Al^{3+}, Mg^{2+}, Ba^{2+}, K^+, Na^+, Pb^{2+}, Co^{2+}, and Mn^{2+}) and anions (SO_3^{2-}, I^-, Br^-, HPO_4^{2-}, and $H_2PO_4^-$). Experiments revealed observable fluorescence property changes only in the

presence of hydrazine, while no other change in the fluorescence property was observed in the presence of other analytes, though Cu^{2+} caused a little interference. The above results showed that probe **24** was highly selective toward hydrazine recognition. The authors utilized probe **24** for the biological imaging of hydrazine inside live HeLa cells and also for detection in the gas phase. They also showed that probe **24** has the potential for practical use in biological and pathological purposes.

Lin and his coworkers developed a highly sensitive colorimetric and ratiometric fluorescent probe **25** for hydrazine detection.[67] With the addition of hydrazine to EtOH–PBS buffer solution (pH 7.2, 10 mM, 9 : 1, v/v) of probe **25**, the absorption band at 344 nm gradually decreased with the simultaneous appearance of a new absorption band at 439 nm, accompanied by a change in the color of the solution from colorless to yellow. Moreover, upon exposure to hydrazine, the fluorescence emission intensity at 467 nm gradually decreased with simultaneous enhancement (15-fold) of the fluorescence emission intensity at 528 nm and the fluorescence color of the solution changed from blue to yellowish green, *i.e.*, the probe showed a ratiometric fluorescence response toward hydrazine and two clear emission peaks were observed before and after the addition of hydrazine. The observed 15-fold enhancement in the fluorescence emission intensity was due to hydrazine-induced phthalimide group deprotection, which released electron-donating free amine groups, facilitating the ICT process. The fluorescence emission intensity ratio ($I_{528\,nm}/I_{467\,nm}$) showed a linear relationship with hydrazine concentration in the range of 0–7.5 μM. The authors also investigated the pH effect of probe **25** by varying the pH ranges. Under acidic conditions (pH 1.0 to 10.0), probe **25** showed blue fluorescence and under strongly basic conditions (pH 12 to 14), probe **25** displayed red fluorescence. It was also noticed that the fluorescence color of the solution after hydrazinolysis, and under strongly basic condition were totally different. From that investigation, it was clear that probe **25** showed a sharp ratiometric fluorescence color change from blue to yellowish green only in the presence of hydrazine in the pH range between 5.0 and 9.0. Thus, the acidic, hydrazinolysis, and basic condition intermediates can be easily isolated depending on the fluorescence color change of the solution and their fluorescence emission intensity values (467, 528, and 596 nm, respectively). This result proved that probe **25** can be used for the imaging of hydrazine inside live cells without any pH interference. Time-dependent photoluminescence measurement showed a variation in the mode of decay of the intermediates. Probe **25** displayed monoexponential fluorescence decay with a lifetime of 4.31 ns, whereas the probe-hydrazine complex displayed biexponential fluorescence decay with a lifetime of 7.91 ns and 1.86 ns, respectively, and the probe-hydroxide complex also showed biexponential fluorescence decay but the lifetimes were 18.38 ns and 2.63 ns, respectively. The drastic change in the lifetime values in the case of the probe hydroxide was due to zwitter-ion formation in strongly basic conditions, whereas the change between the lifetime values is minimal in the case of the probe-hydrazine complex. The different ratiometric color changes in the hydroxide solution (red) and in hydrazinolysis conditions (greenish yellow) were due to the varying nucleophilicity of the analytes. Hence, hydrazine recognition can be done in the presence of bases also. The time-dependent fluorescence study showed that the reaction completed within 15 min and the detection limit of probe **25** was found to be 4.2 nM. The authors utilized probe **25** for the live cell (HeLa cells) imaging of hydrazine.

Li *et al.* synthesized two BODIPY-based fluorescent chemodosimeters (**26** and **27**) for the detection of hydrazine.[68] The addition of hydrazine to the ethanolic aqueous solution (PBS buffer solutions, pH 7.2, 10 mM, 1 : 9, v/v) of probe **26** caused the disappearance of the absorption band at 502 nm with the simultaneous appearance of a new band at 452 nm. A clear isosbestic point at 472 nm indicated the formation of new chemical species. Moreover, the fluorescence emission intensity at 523 nm was increased two-fold with the addition of hydrazine. The fluorescence enhancement was due to the inhibition of the PET process by virtue of the complete hydrazinolysis of the N-protected group. The detection limit of probe **26** was found to be 1.4 μM. On the other hand, upon addition of hydrazine to probe **27**, the absorption band at 507 nm gradually decreased with the formation of a new absorption band with increased absorbance at 430 nm. A clear isosbestic point was observed at 466 nm. Also, on exposure of hydrazine to probe **27** solution, the fluorescence emission intensity decreased about three-fold at 528 nm. The fluorescence quenching was due to an incomplete hydrazinolysis reaction. Here, hydrazine caused an addition reaction, leading to the formation of hydrazide, which induced effective PET operation from hydrazide to the BODIPY fluorophore. The detection limit of probe **27** was found to be 0.18 μM. The authors utilized these probes **26** and **27** for the detection of hydrazine in the aqueous solution (Fig. 19).

2.8. 2-Aza-Cope rearrangement

Aza-Cope rearrangement[69] is a [3,3]-sigmatropic rearrangement reaction of N-substituted 1,6-dienes under heating conditions (Scheme 8). Using this rearrangement reaction, the *N*-substituted 1,6-dienes can be converted to isomerized 3,4-dienes. Cope rearrangement was named after the scientist Cope who discovered the above rearrangement reaction in 1930. After the discovery of Cope rearrangement, Horowitz and Geissman discovered its variant 2-aza-Cope rearrangement.

The addition of formaldehyde to the homoallyl amine gives an iminium ion, which undergoes [3,3]-sigmatropic rearrangement to produce the rearranged iminium ion. The rearranged iminium ion on hydrolysis gives the corresponding aldehyde product (Scheme 9). Based on the above reaction mechanism strategy, a series of formaldehyde responsive fluorescent probes have been developed in the recent years.

In 2015, Chang's group reported a silicon rhodamine-based fluorescent probe **28** containing homoallylamino units.[70] After exposure to formaldehyde, the weakly fluorescent probe turned into a highly red fluorescent one *via* aza-Cope rearrangement. In the presence of formaldehyde at pH 7.4 after 1 h, the fluorescence emission intensity was enhanced about 8-fold at

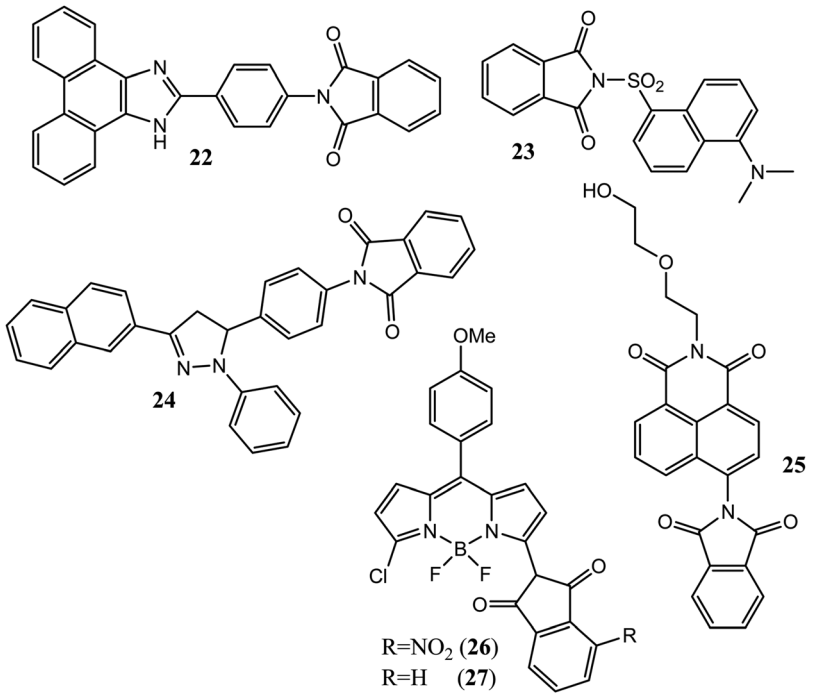

Fig. 19 Chemical structures of hydrazine chemodosimeters **22–27**.

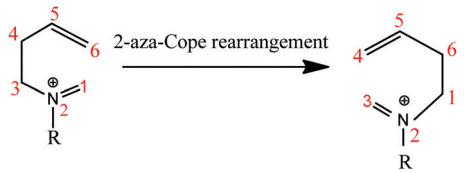

Scheme 8 Plausible mechanism of aza-Cope rearrangement.

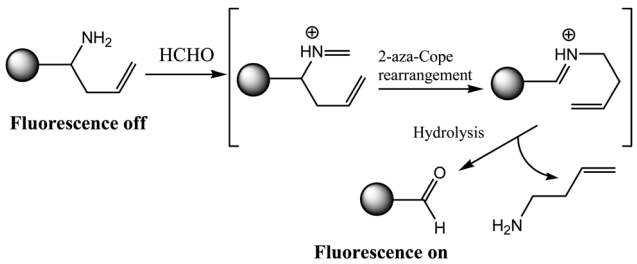

Scheme 9 Plausible reaction mechanism for formaldehyde-selective chemodosimeter based on a 2-aza-Cope rearrangement reaction.

662 nm. They also applied this probe for visualizing the detection of endogenous formaldehyde in MCF7 human breast cancer cells and the exogenous detection of formaldehyde in HEK 293T cells (Fig. 20).

In 2016, Lin and his coworkers developed a ratiometric fluorescent probe **29** for the intracellular detection of formaldehyde.[71] After treatment with formaldehyde, the absorption peak centered at 229 nm decreased and two new absorption peaks centered at 245 nm and 318 nm appeared. The free probe displayed an emission band at 359 nm in a PBS buffer containing 1% acetone. Upon the gradual addition of formaldehyde, the band at 359 nm was red-shifted (about 92 nm) to 451 nm as the homoallylamino group in probe **29**, which was converted to a relatively strong electron withdrawing aldehyde group. Moreover, with the introduction of formaldehyde, a gradual decrease in the emission intensities at 359 nm and concurrently a significant 53.2-fold enhancement in the emission intensities at 451 nm were observed. This is an indication of the switching on the ICT process accompanied by a change in the color of the solution from blue to green. The detection limit of probe **29** for formaldehyde recognition was found to be 5.96×10^{-5} M at pH 7.4 and 1.87×10^{-5} M at pH 4.5, which was much below compared to that at pH 7.4. The above fact was due to the easier formation of the imine intermediates at lower pH, which accelerated the reaction between the probe and the formaldehyde. They also utilized that the probe to detect formaldehyde in HeLa cells (Fig. 21).

Li *et al.* developed *N*,*N*-dimethylquinolin-6-amine fluorescent probe **30** based on the 2-aza-Cope rearrangement reaction.[72] After exposure to formaldehyde, the two major absorption bands at 254 nm and 353 nm showed remarkable bathochromic shifts (23 nm and 76 nm respectively) and two new absorption bands emerged at 277 nm and 429 nm. The probe displayed a broad emission peak at 495 nm. Upon the addition of formaldehyde, the fluorescence intensity at 495 nm gradually decreased with the simultaneous enhancement of fluorescence intensity at 570 nm, indicating the disruption of the ICT process. Moreover, the peak showed a remarkable red shift from 495 nm to 570 nm with a fluorescence color change of the solution from green to yellow. Due to the rearrangement reaction, the homoallylamino group was replaced by a

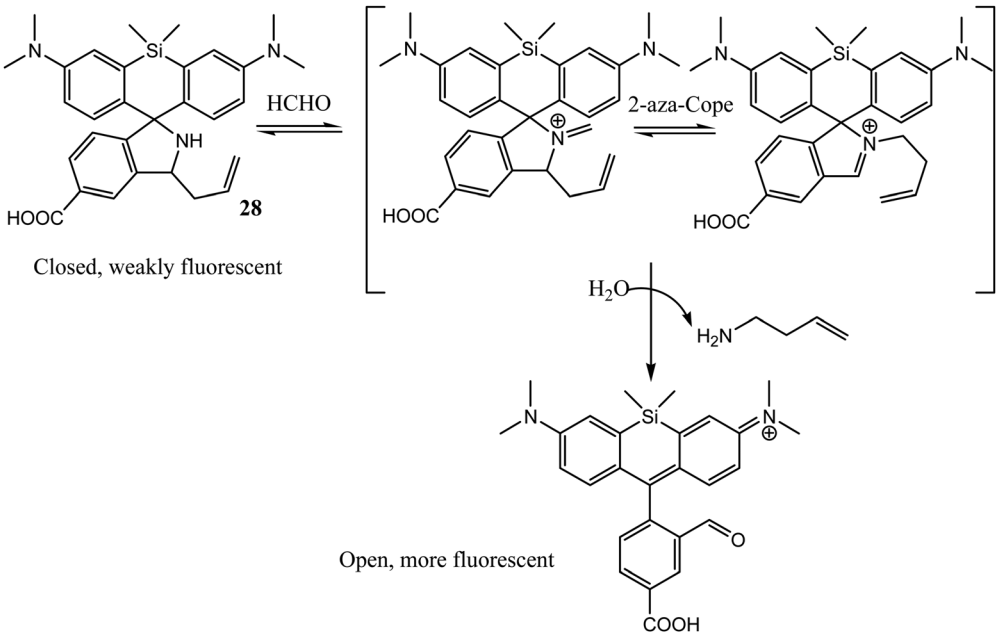

Fig. 20 Reaction mechanism of chemodosimeter **28** with formaldehyde.

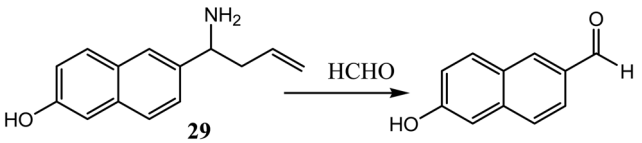

Fig. 21 Chemodosimetric reaction of probe **29** with formaldehyde.

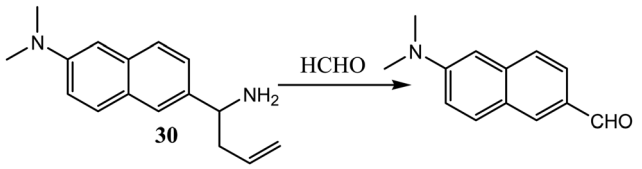

Fig. 22 Chemodosimetric reaction of probe **30** with formaldehyde.

comparatively strong electron withdrawing aldehyde group, which induced such a red shift. The ratio of the fluorescence emission intensities, $I_{570\,nm}/I_{495\,nm}$, showed a 9-fold ratiometric fluorescence enhancement and varied linearly with formaldehyde concentration in the range of 0–200 μM. The detection limit of probe **30** for formaldehyde detection was found to be 0.5 μM. They also applied this ratiometric probe **30** to visualize the detection of exogenous formaldehyde in living *Arabidopsis thaliana* plant tissues. Moreover, probe **30** was utilized to measure formaldehyde levels in different water samples. Furthermore, the authors also developed an easy-to-use test kit for the detection of various concentration formaldehyde in the solution phase (Fig. 22).

Chang's group[73] designed a series of formaldehyde-responsive fluorescent dyes **31–34** based on the *gem*-disubstituent effect at the 4-positions. The authors also showed that the introduction of the *gem*-dimethyl groups at the 4-position triggered aza-Cope rearrangement at a faster rate in the presence of formaldehyde. Moreover, upon exposure to formaldehyde, the emission color of probe **31–34** solution changed from blue to green to orange to red, respectively. The authors also showed that after exposure to formaldehyde for 2 h, probe **31** displayed a 4.5-fold fluorescence turn-on response, whereas in the case of probe **32**, **33**, and **34**, the increase was 2.2-, 10-, and 4-fold, respectively. Confocal microscopic imaging experiments showed when these probes were used for monitoring formaldehyde levels inside the cells (MEF KO and HAPI KO), only the resorufin-based probe **34** scaffold displayed the most red-shifted excitation, emission values, and best fluorescence response compared to the others. The best fluorescence signal of probe **34** was due to its cellular stability and good nuclear staining capacity during the experiment. Consequently, the bioimaging of the probes proved that these probes could be used as indicators for visualizing the detection of exogenous and endogenous formaldehyde in live HEK293T cells. The authors also applied probes **31–34** for detecting the change in the formaldehyde level during cellular metabolism through an enzymatic assay for alcohol dehydrogenase 5 (Fig. 23).

Tang's group reported an acidic pH (4.00–6.00)-activated formaldehyde responsive lysosome-targeted two photon fluorescent probe **35** by linking a napthalimide fragment to the coumarin fluorophore, introducing a 4-(2-ethyl)morpholine unit as a lysosome-targeting group.[74] The authors designed this probe **35** based on the "dual-key-and-one-lock" principle,[75] *i.e.*, in an acidic environment (first key), only the addition of formaldehyde (second key) to the probe **35** triggered 2-aza-Cope rearrangement reaction at the recognition site (lock), releasing coumarin-containing fluorophore. Due to the generation of the coumarin fluorophore, the weak fluorescence emission band at 566 nm caused a blue shift to generate a new fluorescence emission band at 506 nm with enhanced fluorescence emission intensity. Hence, probe **35** showed sensitivity toward formaldehyde

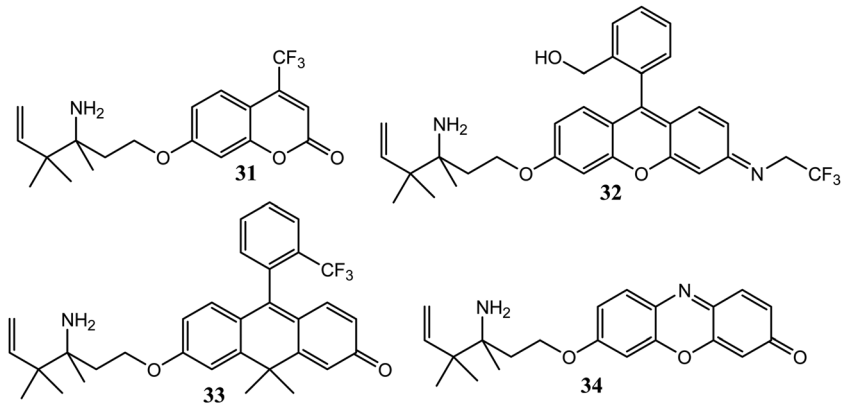

Fig. 23 Chemical structures of formaldehyde recognition chemodosimeters **31–34**.

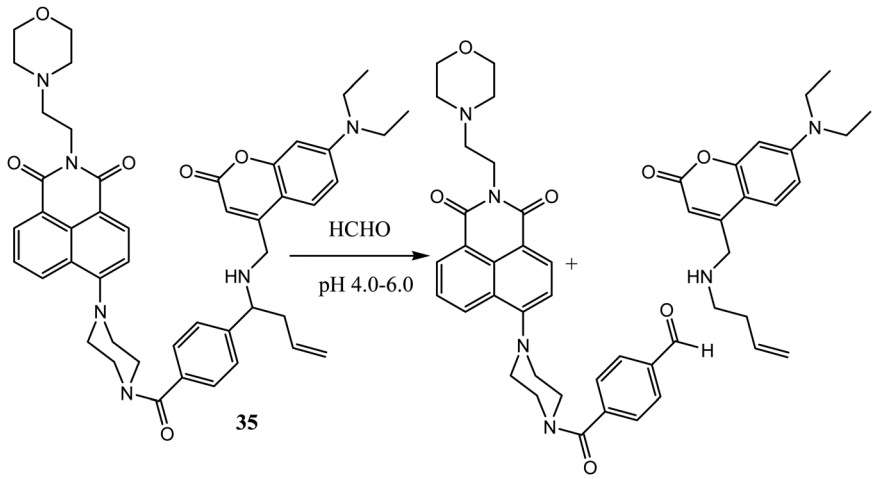

Fig. 24 Chemodosimetric reaction of probe **35** with formaldehyde.

in acidic buffer region (pH 4.0 to 6.0). The detection limit of probe **35** for formaldehyde detection was found to be 3 μM. The main characteristics of probe **35** was that it had the lysosome targeting morpholine unit, which facilitated the accumulation of the probe inside the lysosome, proving its potential ability to detect formaldehyde in lysosome. Furthermore, this work will help researchers to design "dual-key-and-one-lock" probe for the detection of formaldehyde in the acidic microenvironment of lysosome and tumor (Fig. 24).

2.9. Baeyer–Villiger reaction

In 1979, S. Foote and coworkers described the Baeyer–Villiger oxidation, *i.e.*, the reaction mechanism of benzil with H_2O_2, as shown in Scheme 10.[76] The above reaction was named after the German scientist Johann Friedrich Wilhelm Adolf von Baeyer and the Swiss scientist Victor Villiger who discovered it in 1899. The oxidation reaction occurs by the nucleophilic attack of H_2O_2 on the carbonyl carbon of benzil, resulting in the formation of an unstable intermediate, which is then hydrolyzed, generating benzoic acid.

In 2014, Sumimoto's research group developed probe **36** by covalently linking the fluorophore moiety to the SNAP-tag

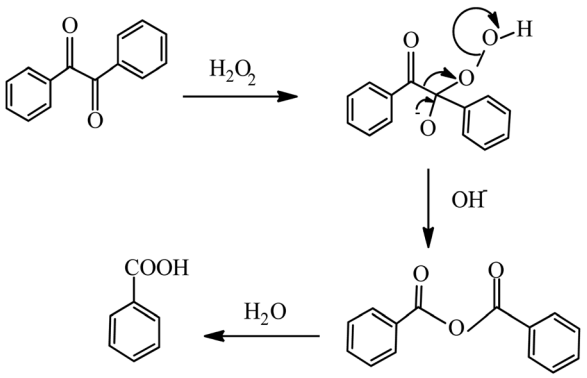

Scheme 10 Plausible mechanism of Baeyer–Villiger oxidation.

protein for H_2O_2 recognition.[77] Probe **36** displayed maximum absorption at 508 nm and maximum emission at 528 nm. The introduction of H_2O_2 to probe **36** caused about 9-fold enhancement of fluorescence red emission intensity at 525 nm. The detection limit of probe **36** for H_2O_2 recognition was found to be 2.0 μM. The kinetic study showed that the reaction between the SNAP-tag protein conjugated to the nitrobenzoyl carbonyl

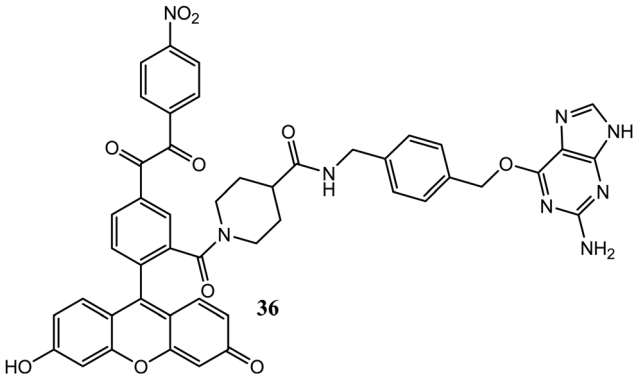

Fig. 25 Chemical structures of the hydrogen peroxide chemodosimeter **36**.

fluorescein fluorophore followed the pseudo-first order kinetics and the rate constant was found to be 6.2×10^{-3} s^{-1}. The probe was successfully applied to detect endogenous H_2O_2 produced during phagocytosis inside RAW264.7 macrophages and exogenous H_2O_2 in living cells such as HEK293T. When the SNAP-tag protein was terminally fused with the transmembrane domain of growth factor PDGFR (Platelet derived growth factor), the tag was expressed outside the plasma membrane. If the HEK293T cells were transfected with SNAP-PDGFR-TM, the SNAP tag was localized on the extracellular surface of the plasma membrane. Thus, the SNAP tag expressing cells were incubated with both H_2O_2 recognition part of the cell and the SNAP surface Alexa Fluor 546. The former gives green emission after reaction with H_2O_2 and the latter is a SNAP tag with red emission. Thus, an enhancement in green fluorescence was noticed after adding exogenous H_2O_2 to these doubly labelled HEK293T cells. In the case of doubly labelled RAW264.7 macrophages, which were incubated with IgG opsonized particles, fluorescence enhancement was seen more effectively in the phagosome membrane than in the plasma membrane, showing the fact that H_2O_2 was mainly produced in the phagosomal membrane (Fig. 25).

Li *et al.* designed two BODIPY probes **37** and **38** for H_2O_2 recognition.[78] The authors reported that both probes **37** and **38** showed the same absorption maxima at 500 nm, which was shifted to 498 nm after reaction with H_2O_2. The emission spectra of both the probes **37** and **38** shifted from 510 nm to 508 nm upon treatment with H_2O_2. The molar absorption coefficients of *m*-nitrobenzil-BODIPY-peroxide and *p*-nitrobenzil-BODIPY-peroxide are 7.34×10^4 M^{-1} cm^{-1} and 6.90×10^4 M^{-1} cm^{-1}, respectively. Moreover, after the addition of H_2O_2, a highly green-emitting fluorescence turn-on response was observed for both the probes. The fluorescence turn-on response was observed because after reaction with H_2O_2 to the benzil recognition moiety, the donor-excited photo-induced electron transfer mechanism (d-PET) restored the fluorescence of both the probes. The investigation showed that in the reaction with excess H_2O_2, the fluorescence intensity of **37** increased 78 times, which is much higher than that of **38**, which increased by 70 times. The above results are due to the **37** (*m*-nitrobenzil BODIPY)

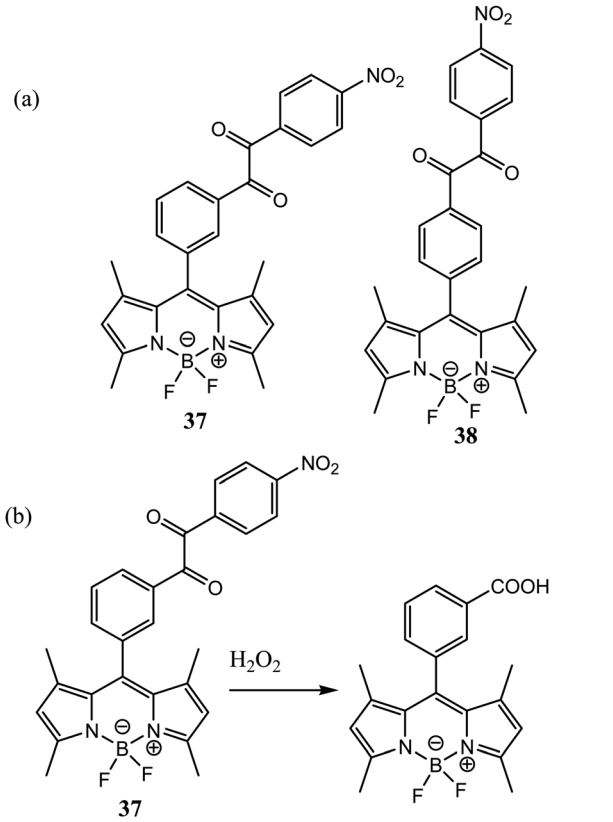

Fig. 26 (a) Chemical structures of hydrogen peroxide chemodosimeters **37** and **38**; (b) chemodosimetric reaction of probe **37** with hydrogen peroxide.

derivative due to the more pronounced steric effect of the carboxy group at the *meta* position of the BODIPY derivative and less electron withdrawing capacity compared to the *para* position of the BODIPY derivative and less electron withdrawing capacity compared to the *para* position of the BODIPY derivative. Probe **37** exhibited high sensitivity (0.94 ppb) and fast response (30 s) to H_2O_2 vapor. The fluorescence intensity at 508 nm showed a good linear relationship with $[H_2O_2]$ in the range of concentration from 10 to 500 ppb. The detection limit of probe **37** for gaseous $[H_2O_2]$ detection was found to be 0.94 ppb. The authors applied probe **37** successfully for the naked eye visual detection of H_2O_2 vapor and live-cell imaging (Fig. 26).

Zhang's group reported the α-keto amide ratiometric fluorescent probe **39** for the selective detection of H_2O_2 in the endoplasmic reticulum.[79] For the addition of H_2O_2 in PBS buffer (20 mM, pH = 7.4, 30% DMSO, v/v), the major absorption peak at 365 nm decreased with the simultaneous appearance of a new absorption peak at 458 nm. The fluorescence emission peak at 465 nm gradually decreased and a new emission peak at 540 nm gradually increased, accompanied by a weak blue fluorescence to strong green fluorescence change. The fluorescence change was after treatment with H_2O_2, and the α-ketoamide probe converted to an amine, a stronger electron donating group. The fluorescence emission intensity ratio ($I_{540}/I_{465\,nm}$) was linearly proportional to the $[H_2O_2]$ concentration in the range of 0–10 μM.

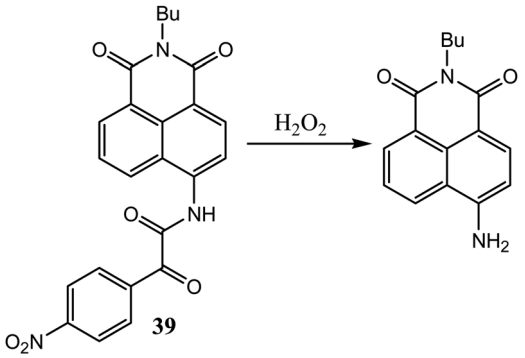

Fig. 27 Chemodosimetric reaction of probe **39** with hydrogen peroxide.

The limit of detection of probe **39** was found to be 37 nM. Probe **39** was used for the quantitative detection of exogenous H_2O_2 in HeLa cells (Fig. 27).

Tang's research group synthesized α-keto amide hemicyanine NIR fluorescent probe **40** for H_2O_2 recognition.[80] Due to good biocompatibility and higher cell permeability, the authors applied this NIR fluorescent probe **40** for mitochondrial localization and the spectral properties of **40** were studied. The authors reported that after the addition of H_2O_2 to the probe, the absorption maxima at 598 nm was shifted to 670 nm with a naked eye color change from blue to blue green. Upon the addition of H_2O_2, the fluorescence emission intensity of **40** at 704 nm rapidly increased and the emission color of the solution changed from colorless to red. It was noticed that near about one-fold fluorescence enhancement was observed due to the liberation of Cy-NH_2 after the addition of H_2O_2, which facilitated the ICT (intramolecular charge transfer) process. Moreover, the fluorescence intensity at 704 nm varied linearly with [H_2O_2] concentration in the range of 0–50 μM. The detection limit of the probe was 26 nM. Probe **40** was applied to monitor the change in the H_2O_2 level during ischemia-reperfusion injury in HepG2 cells and damaged kidneys. The strong fluorescence of the damaged organ was attributed to the presence of a higher concentration of H_2O_2, which induced oxidative damage of the organ. The above experiment proved the probe's potential ability to identify damaged organs inside the body. The authors also injected probe **40** into a Kumming mouse's body to visualize endogenous H_2O_2. They did the experiment by the sequential injection of the probe only, then the probe, rotenone, and finally the probe, rotenone, *N*-acetyl-cysteine into the mouse body. From the fluorescence cell images, they observed that the weak fluorescence signal of the probe suddenly converted to a strong fluorescence signal after the injection of rotenone with the probe into the body and then the fluorescence intensity again decreased after the injection of *N*-acetyl cysteine with the probe and rotenone into the body. They also reported the reason for the observed sequential phenomenon by virtue of rotenone-induced endogenous H_2O_2 formation inside the body and, after that, the scavenging of the produced H_2O_2 with the antioxidant *N*-acetyl cysteine (Fig. 28).

2.10. Beckmann rearrangement

Beckmann rearrangement[81] is a rearrangement reaction where ketoximes undergo acid-catalyzed rearrangement to generate *N*-substituted amides (Scheme 11). The above rearrangement reaction was named after the German scientist Ernst Otto Beckmann who invented the above rearrangement reaction

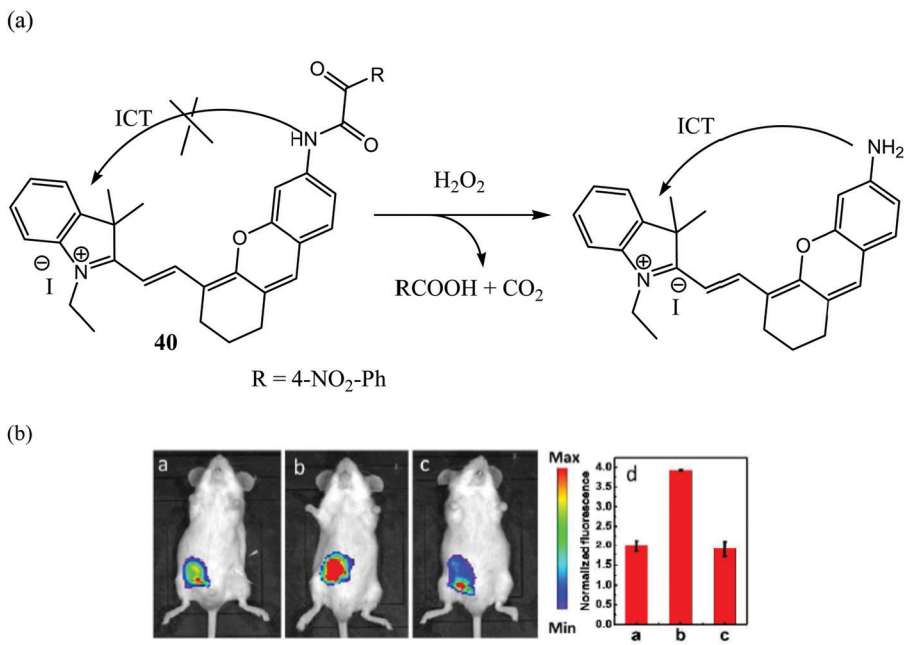

Fig. 28 (a) Chemodosimetric reaction of probe **40** with hydrogen peroxide; (b) fluorescence microscopy images of endogenous H_2O_2 inside mouse body: (a) mouse body injected with **40** only; (b) mouse body injected with rotenone and **40**; (c) mouse body injected with rotenone, *N*-acetyl cysteine, and **40**; (d) relative fluorescence intensity images. Reprinted (adapted) with permission from ref. 80. Copyright (2016) American Chemical Society.

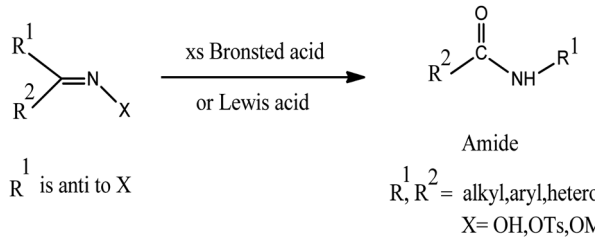

Scheme 11 Plausible mechanism of Beckmann rearrangement.

in 1886. During this rearrangement, the anti-group to the oxime OH migrates to give the *N*-substituted amide as a product. Sometimes, nitrile is also generated as a side product through Beckmann fragmentation, depending on the carbocation stability.

Based on this strategy, Zheng and his coworkers developed a 1,8-napthalimide chromophore-based fluorescent probe **41** for the selective detection of phosgene.[82] In CH_3CN solution, probe **41** displayed three major absorption peaks at 208, 238, and 346 nm. However, after treatment of probe **41** with phosgene, the two former absorption peaks remained unchanged but only the absorption peak centered at 346 nm red shifted to 362 nm. After treatment of probe **41** with 10 μM phosgene, a nearly 260-fold enhancement of the fluorescence intensity at 448 nm was observed with bright blue fluorescence. The turn-on bright blue

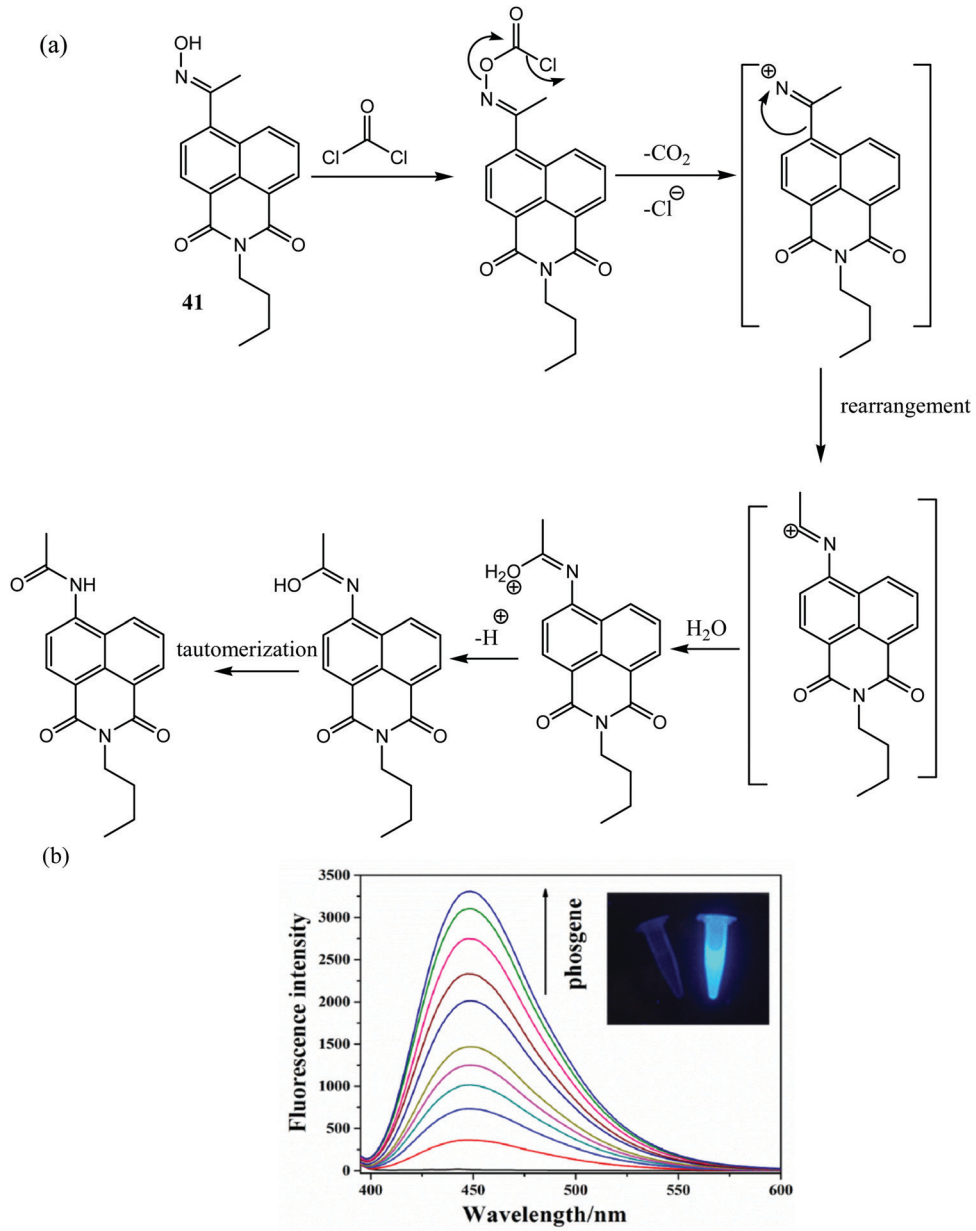

Fig. 29 (a) Reaction mechanism of chemodosimeter **41** with phosgene; (b) fluorescence emission spectra of probe **41** in acetonitrile solution upon the addition of phosgene. Inset: Photographic images of (i) **41** and (ii) **41** + phosgene. Reprinted from ref. 82. Copyright (2020), with permission from Elsevier.

fluorescence was due to the addition of phosgene in acetonitrile solution, which converted the keto–oxime probe **41** to 4-acetamide-1,8-napthalimide through Beckmann rearrangement, *i.e.*, the electron-withdrawing ketoxime group was replaced by an electron-donating acetamido group. The detection limit of probe **41** for phosgene recognition was 6.3 nM. The authors also applied the probe-loaded filter stripe for the successful monitoring of gaseous phosgene (Fig. 29).

2.11. Lossen rearrangement

The thermal base-catalyzed rearrangement of hydroxamic acid or its derivatives to their corresponding isocyanate derivative is known as Lossen rearrangement (Scheme 12).[83] The higher electron donating nature of R and the electron withdrawing nature of R facilitate the reaction to occur at a faster rate. This reaction can be utilized for the conversion of hydroxamate ester to free amine. Lossen rearrangement was named after Wilhelm Lossen, who discovered the above rearrangement reaction in 1872.

Han *et al.* developed a rhodamine–hydroxamate fluorescent probe **42** based on Lossen rearrangement.[84] After the addition of DCP (diethylchlorophosphate) in anhydrous DMF [5% (v/v) water],

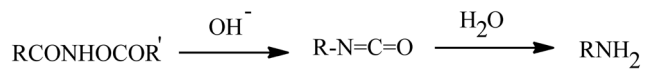

Scheme 12 Plausible mechanism of Lossen rearrangement.

the fluorescence emission intensity at 590 nm gradually increased. The significant turn-on fluorescence response was due to the addition of DCP-induced spirolactum ring opening of the rhodamine fluorophore *via* Lossen rearrangement, which converted the non-fluorescent probe (**42**) to a fluorescent one (**42a**) and the color of the solution changed from colorless to bright red. The time-dependent fluorescence spectra revealed that the reaction completed within 20 min. The detection limit of the probe was 25 ppm. Investigation showed that the reaction was effective in anhydrous medium because of the rapid formation of intermediate **I** compared to phosphate hydrolysis. They also reported that the reaction rate was sufficiently increased in nonpolar solvent, such as DMF, containing a variety of bases, *i.e.*, triethylamine and piperidine. The authors successfully utilized probe **42** for the selective detection of a lower concentration of nerve agents in air (Fig. 30).

Yang *et al.* designed fluorescent probe **43** for the detection of DCP-based *via* the Lossen rearrangement reaction.[85] After exposure to DCP in acetonitrile solution containing triethylamine, the absorption band centered at 248 nm gradually decreased with the simultaneous increase of a new absorption band at 338 nm. Moreover, upon the addition of DCP, the fluorescence emission intensity at 418 nm rapidly increased and the emission color of the solution changed from colorless to blue-violet. The turn-on blue-violet fluorescence was due to the addition of DCP to acetonitrile solution containing triethylamine. The *N*-hydroxy group of probes **43** got phosphorylated to

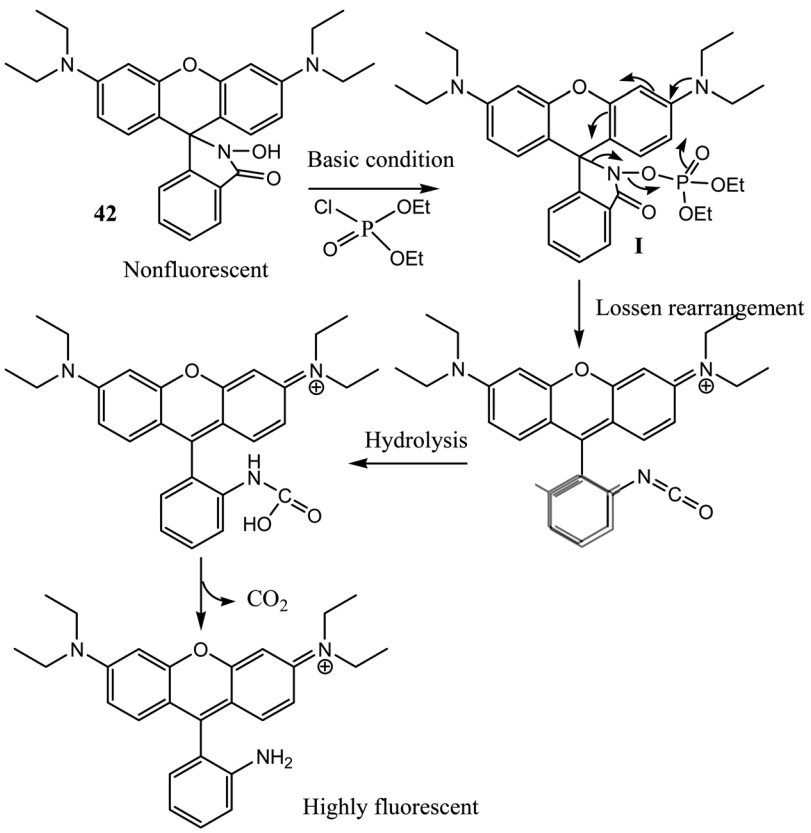

Fig. 30 Plausible DCP sensing mechanism of probe **42**.

Table 1 Summary of the essential photophysical properties and applications of chemodosimeters **1–43**

Probe and analyte	Medium	Detection technique	Sensing mechanism	Excitation	Emissionin presence of analyte	Quantum yield (in absence/in presence of analyte)	Linear Range	Time	Detection limit	Applications	Ref.
Palladium (Pd^0/Pd^{2+}/Pd^{4+}) chemodosimeters											
1 & Pd(0)	CH_3CN : PBS (1 : 3, pH = 7.4, 0.01 M)	Ratiometric, turn-on	—	740 nm↓ and 545 nm↑	825 nm↓ to 655 nm↑	—	0–50 μM	20 min	0.3 ppb	(a) Detection in real water samples and in living cells (HeLa cells). (b) Detection of palladium in aqueous samples by test kits	27
2 & Pd(0)	DMSO : phosphate buffer (1 : 9, v/v, pH = 7)	Turn-on	—	490 nm	—	—	—	80 min	0.1 ppb	Detection of palladium contamination in laboratory.	28
3 & Pd(0)	—	Turn-on	—	—	—	—	—	30 min	—	Detection in mitochondria within HeLa cells	35
4 & Pd(II)/ Pt(IV)	DMSO : pH 10 buffer (1 : 4)	Turn-on	—	—	535 nm	—	For Pd(II) 0.5 to 50 μM	—	3.9 μM (390 ppb) for Pd(II) and 0.54 nM (0.11 ppb) for Pt(IV)	—	37
Cyanide (CN^-) chemodosimeters											
5, **6** & CN^-	**6** MeOH : water (80 : 20)	Turn-on (**6**)	—	—	—	—	—	**6** 1 h	**6** <1.7 μM	—	38 and 39
7 & CN^-	PBS buffer (10 mM, pH 7.4) containing 1% DMSO	Turn-on	—	565 nm	595 nm	—	—	10 s	4 nM	(a) Detection in living cells (HeLa cells) and Blood serum samples. (b) Detection of cyanide in solution by test kits	41
8 & CN^-	Acetonitrile	Turn-on	PET	272 nm	469 nm	—	—	—	1.7 μM	—	43
9, **10** & CN^-	Acetonitrile	Turn-off	—	—	400 (**10**)	0.002/— (**9**), 0.11/— (**10**)	—	Shorter than 10 s (**9**)	—	—	44
11 & CN^-	50% DMSO and HEPES (0.10 M, pH 7.4)	Ratiometric	—	315 nm	350 nm↓ to 518 nm↑	—	—	—	5.3 μM	—	45
Biothiol (cysteine, *N*-acetylcysteine, glutathione, β-mercaptoethanol) chemodosimeters											
12 & Cys	CTAB (cetyl-trimethylammonium bromide) buffer (pH 7.4) and (HEPES buffer, 20 mM)	Turn-on	—	550 nm	621 nm	—	0 to 10 μM	20 min	0.2 μM	Detection in biological media (human plasma samples)	46
13 & cysteine	PBS buffer (20 mM, pH 7.2)	Turn-on	ESIPT	371 nm	415 nm (enol form) 553 nm (keto form)	—/0.45	0 to 30 μM	30 min	0.21 μM	—	47
14, **15** & cysteine	DMSO : H_2O = 7 : 3 v/v, and HEPES buffer, (10 mM, pH = 7.4)	Turn-on	ICT	410 nm	506 nm (**14**)	0.024/— (**14**)	0–100 μM (**14**)	12 min (**14**)	47 ppb (**14**)	Detection in living cells (osteosarcoma MG-63) cells	48

Table 1 (*continued*)

Probe and analyte	Medium	Detection technique	Sensing mechanism	Excitation	Emissionin presence of analyte	Quantum yield (in absence/in presence of analyte)	Linear Range	Time	Detection limit	Applications	Ref.
16 & cysteine	DMSO : PBS buffer (1 : 1 v/v, pH = 7.4, 10 mM)	Turn-on	—	560 nm	706 nm	—	0 μM to 10 μM	30 min	81 nM	Detection in living cells (HeLa cells)	49
17 & cysteine	Acetonitrile : water = 1 : 9 v/v, and PBS buffer, (50 mM, pH = 7.0)	Turn-on	ICT	490 nm	554 nm	$<1 \times 10^{-4}$/ 2.4	0 μM to 70 μM	15 min	1.2×10^{-7} M	Detection in living cells (HeLa cells)	58
18 & thiols (NAC)	0.1 M sodium phosphate buffer (pH = 7.4) containing 0.1% DMSO as the cosolvent	Turn-on	PET	505 nm	—	0.002/0.73	—	—	—	Detection of bovine-serum albumin (BSA).	59
19 & thiols	Tris–HCl buffer (50 mM; pH 7.4)	Turn-on	ICT	400 nm (GSH)	465 nm (GSH)	0.001/0.47 (GSH)	0 nM to 100 nM (GSH)	<1 min (Cys)	<0.5 nM (GSH)	(a) Detection of quantity of thiols in living cells (HEK-293 cell) (b) Control of cytosolic GSH level through glutathione reductase enzymatic essay.	60
Hydrazine (N_2H_4) chemodosimeters											
20 & hydrazine	Water : DMSO (4 : 6, v/v)	Turn-on	—	420 nm	540 nm	—	1–50 μM	100 s	8.8×10^{-9} M (0.3 ppb)	Detection in (a) living cells (HeLa cells) and (b) vapor phase by test kits.	62
21 & hydrazine	H_2O : DMSO (4 : 6, v/v) and HEPES buffer (10 mM, pH = 7.4).	Turn-on	PET	313 nm	498 nm	0.067/0.704	0.025 μM to 1.5 μM	20 min	8.47×10^{-8} M (2.9 ppb)	Detection in (a) living cells (Vero 76 cells) and (b) vapor phase by test kits.	63
22 & hydrazine	0.4 mM TX-100 in HEPES buffer (10 mM, pH = 7.2)	Turn-on	—	360 nm	430 nm	0.008/0.473	0 μM to 30 μM	40 min	1.5 ppb	Detection in (a) living cells (HepG2 cells), (b) *in vitro* assay for aminoacylase-1.	64
23 & hydrazine	HEPES buffer (pH 7.0, 20 mM) : DMSO (1 : 9, v/v)	Turn-on	—	353 nm	512 nm	0.093/0.498	0 μM to 5 μM	1 h	1.88×10^{-7} M (6.01 ppb)	Detection in (a) living cells (HeLa cells) and (b) vapor phase by test kits.	65
24 & hydrazine	PBS buffer (10 mM, pH 7.4) containing 30% CH_3CN	Turn-on	PET	370 nm	490 nm	—	10 μM to 20 μM	4 min	0.0622 μM (1.99 ppb)	Detection in (a) living cells (HeLa cells) and (b) vapor phase.	66
25 & hydrazine	PBS buffer (10 mM, pH 7.2) : EtOH (1 : 9, v/v)	Ratiometric	ICT	405 nm	467 nm↓ to 528 nm↑	—	0 μM to 7.5 μM	15 min	4.2 nM	Detection in living cells (HeLa cells).	67
26, **27** & hydrazine	DMSO : water (9 : 1, v/v)	Turn-on Turn-off (**26**)	PET		523 nm (**25**) 528 nm (**26**)	—	—	20 min (**25**) 5 min	1.4 μM (**25**) 0.18 μM (**26**)	—	68
Formaldehyde (HCHO) chemodosimeters											
28 & formaldehyde	PBS buffer (20 mM, pH = 7.4)	Turn-on	—	645 nm	662 nm	0.36/—	—	1 h	5 μM	Detection of (a) formaldehyde in living (HEK293T) cell. (b) Endogenous formaldehyde in live (MCF7 human breast cancer) cell.	70

Table 1 (*continued*)

Probe and analyte	Medium	Detection technique	Sensing mechanism	Excitation	Emissionin presence of analyte	Quantum yield (in absence/in presence of analyte)	Linear Range	Time	Detection limit	Applications	Ref.
29 & formaldehyde	PBS buffer (25 mM); containing 1% acetone (pH 7.4 or 4.5)	Ratiometric	ICT	318 nm	359 nm↓ to 451 nm↑	0.015/0.029	—	200 min	5.96×10^{-5} M at pH 7.4, 1.87×10^{-5} M at pH 4.5	Detection in living cells (HeLa cells).	71
30 & formaldehyde	PBS buffer (10 mM; pH = 7.4) containing 1% acetonitrile	Ratiometric	ICT	405 nm	495 nm↓ to 570 nm↑	—	0 μM to 200 μM	120 min	0.5 μM	(a) Detection of exogenous and endogenous formaldehyde in living *Arabidopsis thaliana* plant tissues. (b) Test kits	72
31–34 & formaldehyde	PBS buffer (20 mM; pH = 7.4)	Turn-on	—	385 (**31**)	498 (**31**)	0.11/— (**31**)	—	2 h	10 μM	Detection of (a) changes in the level of formaldehyde during cellular metabolism through invitro assay for alcohol dehydrogenase 5 in (MEFKO and HAPIKO) cells.	73
				498 (**32**)	515 (**32**)	0.23/— (**32**)				(b) Detection in live (HEK293T) cells.	
				555 (**33**)	572 (**33**)	0.50/— (**33**)					
				573 (**34**)	585 (**34**)	0.18/— (**34**)					
35 & formaldehyde	Phosphate buffer (50 mM, pH = 5)	Turn-on	—	405 nm	506 nm	—	—	—	3 μM	Detection in lysosome and tumor	74
Hydrogen peroxide (H_2O_2) chemodosimeters											
36 & H_2O_2	Phosphate buffer (100 mM; pH = 7.4)	Turn-on	PET	505 nm	525 nm	0.028/—	—	—	2 μM	Detection of (a) exogenous peroxide in living (HEK293T) cell. (b) Endogenous peroxide inside (RAW264.7) phagosomes during phagocytosis	77
37, **38** & H_2O_2	1.0 μM aqueous solution containing 20% CH_3CN = 7.4	Turn-on	PET	480 nm (**37** & **38**)	508 nm	0.010/0.56 (**37**) 0.008/0.43 (**38**)	1 to 100 μM (**37**)	30s (**37**)	0.16 μM (0.94 ppb) (**37**)	Detection in (a) living cells (HeLa cells) and (b) vapor phase (**37**)	78
39 & H_2O_2	DMSO : PBS buffer (3 : 7, v/v 20 mM, pH = 7.4)	Ratiometric	—	395 nm	465 nm↓ to 540 nm↑	—	0 μM to 10 μM	—	38 nM	Detection of endogenous peroxide in endoplasmic reticulum in living (HeLa) cells.	79
40 & H_2O_2	PBS buffer (50 mM, pH 7.4) with 1% methanol	Turn-on	ICT	670 nm	704 nm	0.066/0.636	0 μM to 50 μM	10 min	26 nM	Detection of endogenous H_2O_2 in mitochondria in living (HepG2) cell, kidney during ischemia reperfusion injury and *in vivo* studies in mice	80

Table 1 (*continued*)

Probe and analyte	Medium	Detection technique	Sensing mechanism	Excitation	Emissionin presence of analyte	Quantum yield (in absence/in presence of analyte)	Linear Range	Time	Detection limit	Applications	Ref.
Phosgene ($COCl_2$) chemodosimeter											
41 & phosgene	Acetonitrile solution	Turn-on	ICT	367 nm	448 nm	—	0 μM to 10 μM	15 min	6.3 nM	Detection in vapor phase by test stripes.	82
Diethyl chlorophosphate (DCP) chemodosimeters											
42 & DCP	DMF-containing triethylamine (3%,v/v)	Turn-on	—	560 nm	590 nm	—	—	20 min	25 ppm	—	84
43 & DCP	Acetonitrile solution	Turn-on	ICT	330 nm	418 nm	0.0001/0.2533	0 μM to 20 μM	100 s	10.4 nM	Detection of DCP vapor using test strips.	85

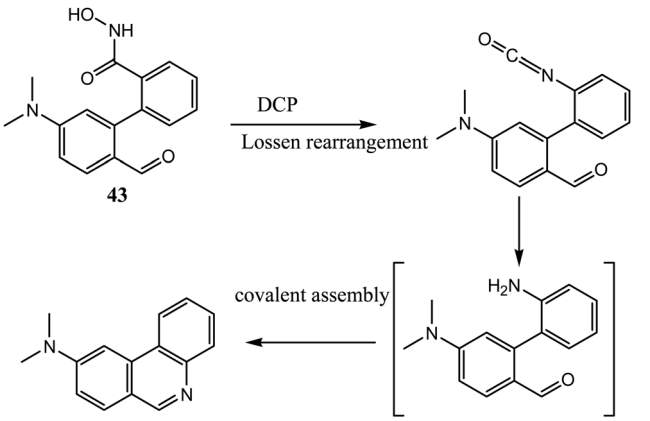

Fig. 31 Plausible DCP sensing mechanism of probe **43**.

form a phosphoryl derivative, which, *via* Lossen rearrangement, generated isocyanate and aniline intermediates sequentially and the aniline intermediate again through intramolecular covalent association, which yielded a highly fluorescent phenanthrene molecule. Furthermore, the fluorescence intensity at 418 nm varied linearly with [DCP] concentration in the range of 0–20 μM. The detection limit of probe **43** was 10.4 nM. The time-dependent fluorescence response study showed that the reaction completed within 100 s. The fluorescence quantum yield of probe **43** before and after the addition of DCP was 0.0001 and 0.2533, respectively (Table 1). The authors applied probe **43** successfully for the detection of DCP vapor using handy test kits (Fig. 31).

3. Conclusion and perspective

This review highlights the studies of various types of fluorescent probes based on different types of name reactions taking place at the molecular recognition site. The main interest of this review is to show different name reaction-based approach for designing various types of fluorescent probes for analyte recognition. The reported fluorescent probes involve 11 types of name reactions, which occur between the receptor and the analyte.

- Tsuji–Trost allylic cleavage-based approach can be used in the development of NIR ratiometric cell permeable fluorescent probe. The mechanism lies behind the fact that Pd^{2+}-induced allylic carbamate/allylic–ether bond cleavage leads to a variation in the conjugate chain length, changing the optical properties of the probe.
- Pd-catalyzed Suzuki–Miyaura coupling reaction results in the formation of highly fluorescent extended conjugated moiety. This mechanism helps in the intracellular detection of Pd(0) within the HeLa cells.
- Claisen rearrangement-based fluorescent probes help in the detection of Pd(II) and Pt(IV) species in contaminated water.
- Benzil-cyanide reaction-based approaches are helpful for the design of rapid responsive cyanide sensing turn-on fluorescent probes though cyanide-mediated benzil bond cleavage

disrupting π-conjugation and the detection limit of cyanide detection for such probes is very low.

• Intramolecular-crossed benzoin condensation reaction-based approaches are helpful to design ratiometric fluorescent probes, followed by cyanohydrin formation and intramolecular nucleophilic attack of cyanohydrin to another carbonyl of the same molecule.

• Michael reaction-based approach for cyanide recognition shows strong turn on-fluorescence response by the conversion of the keto form into the enol form. Moreover, Michael addition-based approach for the recognition of thiols to the maleimide moiety helps to design PET quenching turn-on fluorescent probe. Also, cysteine-triggered acryloyl moiety cleavage helps to develop turn-on fluorescent probe through the intramolecular cyclization of seven-membered ring formation; this approach is also helpful for the detection of cysteine in biological samples and in live cell imaging.

• In the Gabriel mechanism, hydrazine recognition occurs through the hydrolysis of *N*-substituted phthalimide group, resulting in a significant turn-on fluorescence response.

• In some of aza-Cope rearrangement-based formaldehyde responsive fluorescent probes, ratiometric fluorescence response occurs due to the presence of free NH_2 group at the allylic position; moreover, the presence of the *gem* diethyl substituents at the allylic position triggered faster rate of fluorescence response compared to the others. These points should be remembered during the design of such probes.

• There also mentioned keto amide-based probes, which give turn-on fluorescence response through Baeyer–Villiger oxidation, generating corresponding carboxylic acids. These methods are generally used to detect intracellular H_2O_2 in live cells.

• In Beckmann rearrangement-based approaches, ketoxime probes rearrange to its *N*-substituted amides in the presence of phosgene. Because of the substitution of the electron withdrawing ketoxime group by the electron donating acetamide group, significant turn-on fluorescence response was observed.

• Through Lossen rearrangement, hydroxamate probes rearrange to form amine with significant turn-on fluorescence response. This rearrangement technique has been utilized in DCP vapor detection.

The different name reaction-based approaches described here help to design suitable reactive probes with specific sensitivity.

Despite achieving success, many issues are still present in this field.

• The different fluorescent chemodosimeters reported here are mostly turn on/turn off fluorescence response probes. But signal interference by several external factors, *i.e.*, temperature, pH, unknown concentration of analytes, and light source fluctuation may, cause errors in fluorescence intensity measurement. Comparatively, dual emission intensity ratio-based ratiometric fluorescent probes give more accurate fluorescent intensity measurement without any signal interference.

• Though few ratiometric fluorescent probes have been reported, the number of NIR-based fluorescent probes are very few. NIR-based fluorescent probes have high advantages over other fluorescent probes due to longer wavelength, deep tissue penetration, minimum tissue damage, and very low signal interference. Due to these advantages, NIR-based fluorescent probes are also useful for biological imaging. Thus, from these benefits, researchers can gain some insights into the design of NIR probes using name reaction-based approaches in the future.

• Though many fluorescent probes reported in this review have practical application in aqueous solution and live cell imaging, there are a few probes that have no practical implementation. Thus, while designing these probes, researchers should keep the fact in mind that the probes should be water soluble for use in live cell imaging and drinking water. The water solubility of these probes can be improved by incorporating hydrophilic groups, *i.e.*, sulfonate, phosphate, and hydroxide to the water insoluble fluorophore core such as BODIPY and binaphthol.

• Various types of probes reported in this review have been used for diagnosis purposes. However, there are also some limitations. Most of the probes have been used *in vitro*, in cell culture, or in cell imaging studies; however, there are relatively few probes that have been used *in vivo* or for clinical diagnosis. For *in vivo* studies, the fluorophore molecules must be quite stable and easily excreted from the body. But unfortunately, except for rhodamine derivatives, other derivatives, *i.e.*, fluorescein, BODIPY, and other cyanine derivatives, rapidly lose their fluorescence within days. Not only the fluorophore but the stability of the linkage is also important. The linkage by which the fluorophore molecule is conjugated to the targeting moiety should be metabolized slowly. As a result, the length of the conjugated linkage chain must be increased. The chosen fluorophore molecule must be sufficiently brighter and its wavelength should be in the NIR region so that it can penetrate the tissue deeply and cause a higher signal-to-noise ratio, which lowers the background signal.[86] Thus, researchers should focus on designing more NIR probes in the future for better *in vivo* imaging. The molecular weight of the fluorophore molecules should be low enough to activate enzyme catalysis and show sensitivity in particular environments (*i.e.*, in acidic environments). For that purpose, the researchers will also design pH-sensitive fluorescent probes that change fluorescence in the acidic pH region (in cancer cells, tumors, *etc.*). Researchers should give emphasis to design particular targeting moieties (*i.e.*, lysosome, mitochondria, and endoplasmic reticulum) conjugated fluorophores in the future for *in vivo* cell imaging.

• Furthermore, there are different types of sensing mechanisms, *i.e.*, PET, ICT, and ESIPT, that have been reported in this literature survey. Other sensing mechanisms such as AIE (aggregation-induced emission), TBET (through-bond energy transfer), TSCT (through-space charge transfer),[87,88] C=N bond isomerization, excimer, and exciplex formation also needs future investigation.

We think that this review will motivate researchers to design new fluorescent probes with new analytes through new and unexplored reaction-based approach in the future.

Conflicts of interest

The authors declare no conflict of interest for this manuscript.

Acknowledgements

AM and DB thanks CSIR, New Delhi, India [File No.: 08/003(0139)/2019-EMR-I and 08/003(0143)/2020-EMR-I for AM and DB, respectively] for a fellowship.

References

1 C. J. Pedersen, *Angew. Chem., Int. Ed. Engl.*, 1988, **27**, 1021.
2 J.-M. Lehn, *Angew. Chem., Int. Ed. Engl.*, 1988, **27**, 89.
3 C. J. Pedersen, *J. Am. Chem. Soc.*, 1967, **89**, 2495.
4 J. M. Lehn, *Proc. Natl. Acad. Sci. U. S. A.*, 2002, **99**, 4763.
5 C. J. Pedersen, *J. Am. Chem. Soc.*, 1967, **89**, 7017.
6 M. Wenzel, J. R. Hiscock and P. A. Gale, *Chem. Soc. Rev.*, 2012, **41**, 480.
7 E. V. Anslyn, *J. Org. Chem.*, 2007, **72**, 687.
8 P. A. Gale, *Chem. Soc. Rev.*, 2010, **39**, 3746.
9 X. Lou, D. Ou, Q. Li and Z. Li, *Chem. Commun.*, 2012, **48**, 8462.
10 I. V. Kolesnichenko and E. V. Anslyn, *Chem. Soc. Rev.*, 2017, **46**, 2385.
11 L. A. Joyce, S. H. Shabbir and E. V. Anslyn, *Chem. Soc. Rev.*, 2010, **39**, 3621.
12 A. W. Czarnik, *Fluorescent Chemosensors for Ion and Molecule Recognition*, American Chemical Society, Washington, DC, 1993.
13 A. W. Czarnik, *Acc. Chem. Res.*, 1994, **27**, 302.
14 D. Wu, A. C. Sedgwick, T. Gunnlaugsson, E. U. Akkaya, J. Yoon and T. D. James, *Chem. Soc. Rev.*, 2017, **46**, 7105.
15 Y. Yang, Q. Zhao, W. Feng and F. Li, *Chem. Rev.*, 2013, **113**, 192.
16 J. Du, M. Hu, J. Fan and X. Peng, *Chem. Soc. Rev.*, 2012, **41**, 4511.
17 D. T. Quang and J. S. Kim, *Chem. Rev.*, 2010, **110**, 6280.
18 K. Kaur, R. Saini, A. Kumar, V. Luxami, N. Kaur, P. Singh and S. Kumar, *Coord. Chem. Rev.*, 2012, **256**, 1992.
19 M.-Y. Chae and A. W. Czarnik, *J. Am. Chem. Soc.*, 1992, **114**, 9704.
20 M. E. Jun, B. Roy and K. H. Ahn, *Chem. Commun.*, 2011, **47**, 7583.
21 T. L. Mako, J. M. Racicot and M. Levine, *Chem. Rev.*, 2019, **119**, 322.
22 D. Cao, Z. Liu, P. Verwilst, S. Koo, P. Jangili, J. S. Kim and W. Lin, *Chem. Rev.*, 2019, **119**, 10403.
23 D. Banik, S. K. Manna and A. K. Mahapatra, *Spectrochim. Acta, Part A*, 2021, **246**, 119047.
24 S. K. Manna, T. K. Achar and S. Mondal, *Anal. Methods*, 2021, **13**, 1084.
25 S. K. Manna, A. Gangopadhyay, K. Maiti, S. Mondal and A. K. Mahapatra, *ChemistrySelect*, 2019, **4**, 7219.
26 K. J. Bonney and F. Schoenebeck, *Chem. Soc. Rev.*, 2014, **43**, 6609.
27 X. Wang, Z. Guo, S. Zhu, H. Tian and W. Zhu, *Chem. Commun.*, 2014, **50**, 13525.
28 D. Li, L. D. Campbell, B. A. Austin and K. Koide, *ChemPlusChem*, 2012, **77**, 281.
29 F. S. Han, *Chem. Soc. Rev.*, 2013, **42**, 5270.
30 A. J. J. Lennox and G. C. Lloyd-Jones, *Chem. Soc. Rev.*, 2014, **43**, 412.
31 R. Balamurugan, J.-H. Liu and B.-T. Liu, *Coord. Chem. Rev.*, 2018, **376**, 196.
32 T. Wang, N. Zhang, W. Bai and Y. Bao, *Polym. Chem.*, 2020, **11**, 3095.
33 P. Chen, W. Bai and Y. Bao, *J. Mater. Chem. C*, 2019, **7**, 11731.
34 L. Kurti and B. Czako, *Strategic Applications of Named Reactions in Organic Synthesis*, Elsevier Academic Press, Amsterdam, 2005.
35 R. M. Yusop, A. Unciti-Broceta, E. M. V. Johansson, R. M. Sanchez-Martin and M. Bradley, *Nat. Chem.*, 2011, **3**, 239.
36 K. Hiratani and M. Albrecht, *Chem. Soc. Rev.*, 2008, **37**, 2413.
37 A. L. Garner and K. Koide, *J. Am. Chem. Soc.*, 2008, **130**, 16472.
38 D.-G. Cho, J. H. Kim and J. L. Sessler, *J. Am. Chem. Soc.*, 2008, **130**, 12163.
39 J. L. Sessler and D.-G. Cho, *Org. Lett.*, 2008, **10**, 73.
40 Y. Hachisu, J. W. Bode and K. Suzuki, *J. Am. Chem. Soc.*, 2003, **125**, 8432.
41 J. H. Lee, J. H. Jang, N. Velusamy, H. S. Jung, S. Bhuniya and J. S. Kim, *Chem. Commun.*, 2015, **51**, 7709.
42 Y. Zhang and W. Wang, *Stereosel. Organocatal.*, 2013, 147.
43 S. Park and H. J. Kim, *Chem. Commun.*, 2010, **46**, 9197.
44 Y. Sun, Y. Wang, D. Cao, H. Chen, Z. Liu and Q. Fang, *Sens. Actuators, B*, 2012, **174**, 500.
45 H. Lee and H. J. Kim, *Tetrahedron Lett.*, 2012, **53**, 5455.
46 X. Yang, Y. Guo and R. M. Strongin, *Org. Biomol. Chem.*, 2012, **10**, 2739.
47 Y. Zhang, J. H. Wang, W. Zheng, T. Chen, Q. X. Tong and D. Li, *J. Mater. Chem. B*, 2014, **2**, 4159.
48 S. Manna, P. Karmakar, S. S. Ali, U. N. Guria, S. K. Samanta, R. Sarkar, P. Datta and A. K. Mahapatra, *Anal. Methods*, 2019, **11**, 1199.
49 D. Yu, Q. Zhang, S. Ding and G. Feng, *RSC Adv.*, 2014, **4**, 46561.
50 J. Mariam, A. H. Ashoka, V. Gaded, F. Ali, H. Malvi, A. Das and R. Anand, *Org. Biomol. Chem.*, 2021, **19**, 5161.
51 H. Agarwalla, H. A. Anila, F. Ali, S. R. Pradhan, B. Ganguly, S. K. Pramanik and A. Das, *Chem. Commun.*, 2018, **54**, 9079.
52 F. Ali, H. A. Anila, N. Taye, R. G. Gonnade, S. Chattopadhyay and A. Das, *Chem. Commun.*, 2015, **51**, 16932.
53 H. A. Anila, U. G. Reddy, F. Ali, N. Taye, S. Chattopadhya and A. Das, *Chem. Commun.*, 2015, **51**, 15592.
54 U. G. Reddy, H. Agarwalla, N. Taye, S. Ghorai, S. Chattopadhyay and A. Das, *Chem. Commun.*, 2014, **50**, 9899.
55 H. Singh, K. Tiwari, R. Tiwari, S. K. Pramanik and A. Das, *Chem. Rev.*, 2019, **119**, 11718.
56 A. H. Ashoka, F. Ali, S. A. Kushwaha, N. Taye, S. Chattopadhyay and A. Das, *Anal. Chem.*, 2016, **88**, 12161.
57 J. E. T. Corrie, *J. Chem. Soc., Perkin Trans. 1*, 1994, 2975.
58 Y. Shen, C. Liu, Y. Zhang, X. Zhang, C. Zhang, J. Jin, X. Liu, H. Li and S. Yao, *Anal. Methods*, 2015, **7**, 6419.

59 T. Matsumoto, Y. Urano, T. Shoda, H. Kojima and T. Nagano, *Org. Lett.*, 2007, **9**, 3375.
60 L. Yi, H. Li, L. Sun, L. Liu, C. Zhang and Z. Xi, *Angew. Chem., Int. Ed.*, 2009, **48**, 4034.
61 S. Gabriel, *Ber. Dtsch. Chem. Ges.*, 1887, **20**, 2224.
62 L. Cui, Z. Peng, C. Ji, J. Huang, D. Huang, J. Ma, S. Zhang, X. Qian and Y. Xu, *Chem. Commun.*, 2014, **50**, 1485.
63 R. Maji, A. K. Mahapatra, K. Maiti, S. Mondal, S. S. Ali, P. Sahoo, M. R. Uddin, S. Goswami, C. K. Quah and H. K. Fun, *RSC Adv.*, 2016, **6**, 70855.
64 F. Ali, H. A. Anila, N. Taye, D. G. Mogare, S. Chattopadhyay and A. Das, *Chem. Commun.*, 2016, **52**, 6166.
65 X. X. Zhao, J. F. Zhang, W. Liu, S. Zhou, Z. Q. Zhou, Y. H. Xiao, G. Xi, J. Y. Miao and B. X. Zhao, *J. Mater. Chem. B*, 2014, **2**, 7344.
66 L. Wanga, F. Y. Liu, H. Y. Liu, Y. S. Dong, T. Q. Liu, J. F. Liu, Y. W. Yao and X. J. Wan, *Sens. Actuators, B*, 2016, **229**, 441.
67 M. V. R. Raju, E. C. Prakash, H. C. Chang and H. C. Lin, *Dyes Pigm.*, 2014, **103**, 9.
68 B. Li, Z. He, H. Zhou, H. Zhang, W. Li, T. Cheng and G. Liu, *Dyes Pigm.*, 2017, **146**, 300.
69 L. E. Overman, L. T. Mendelson and E. J. Jacobsen, *J. Am. Chem. Soc.*, 1983, **105**, 6629.
70 T. F. Brewer and C. J. Chang, *J. Am. Chem. Soc.*, 2015, **137**, 10886.
71 L. He, X. Yang, Y. Liu, X. Kong and W. Lin, *Chem. Commun.*, 2016, **52**, 4029.
72 Z. Li, Y. Xu, H. Zhu and Y. Qian, *Chem. Sci.*, 2017, **8**, 5616.
73 K. J. Bruemmer, R. R. Walvoord, T. F. Brewer, G. B. Barragan, N. Wit, L. B. Pontel, K. J. Patel and C. J. Chang, *J. Am. Chem. Soc.*, 2017, **139**, 5338.
74 X. Xie, F. Tang, X. Shangguan, S. Che, J. Niu, Y. Xiao, X. Wang and B. Tang, *Chem. Commun.*, 2017, **53**, 6520.
75 H. Feng, Q. Meng, H. T. Ta and R. Zhang, *New J. Chem.*, 2020, **44**, 12890.
76 Y. Sawaki and C. S. Foote, *J. Am. Chem. Soc.*, 1979, **101**, 6292.
77 M. Abo, R. Minakami, K. Miyano, M. Kamiya, T. Nagano, Y. Urano and H. Sumimoto, *Anal. Chem.*, 2014, **86**, 5983.
78 B. Li, J. B. Chen, Y. Xiong, X. Yang, C. Zhao and J. Sun, *Sens. Actuators, B*, 2018, **268**, 475.
79 C. Gao, Y. Tian, R. B. Zhang, J. Jing and X. Zhang, *Anal. Chem.*, 2017, **89**, 12945.
80 X. Xie, X. Yang, T. Wu, Y. Li, M. Li, Q. Tan, X. Wang and B. Tang, *Anal. Chem.*, 2016, **88**, 8019.
81 L. Field, P. B. Hughmark, S. H. Shumaker and W. S. Marshall, *J. Am. Chem. Soc.*, 1961, **83**, 1983.
82 Y. L. Huang, W. Ye, Y. T. Su, Z. Y. Wu and H. Zheng, *Dyes Pigm.*, 2020, **173**, 107854.
83 C. J. Salomon and E. Breuer, *J. Org. Chem.*, 1997, **62**, 3858.
84 S. Han, Z. Xue, Z. Wang and T. B. Wen, *Chem. Commun.*, 2010, **46**, 8413.
85 B. Huo, M. Du, A. Shen, M. Li, Y. Lai, X. Bai, A. Gong and Y. Yang, *Anal. Chem.*, 2019, **91**, 10979.
86 H. Kobayashi, M. Ogawa, R. Alford, P. L. Choyke and Y. Urano, *Chem. Rev.*, 2010, **11**, 2620.
87 J. Hu, Q. Li, X. Wang, S. Shao, L. Wang, X. Jing and F. Wang, *Angew. Chem., Int. Ed.*, 2019, **58**, 8405.
88 S. Ye, T. Tian, A. J. Christofferson, S. Erikson, J. Jagielski, Z. Luo, S. Kumar, C.-J. Shih, J.-C. Leroux and Y. Bao, *Sci. Adv.*, 2021, **7**, eabd1794.

